NASA Contractor Report 4151

Characterization of Noncontact Piezoelectric Transducer With Conically Shaped Piezoelement

James H. Williams, Jr., and Simeon C. U. Ochi

FOR REFERENCE

NASA

NF01828

NASA Contractor Report 4151

Characterization of Noncontact
Piezoelectric Transducer With
Conically Shaped Piezoelement

James H. Williams, Jr., and Simeon C. U. Ochi
Massachusetts Institute of Technology
Cambridge, Massachusetts

ΝΛSΛ

National Aeronautics
and Space Administration

Scientific and Technical
Information Division

1988

ABSTRACT

In this report, the characterization of a dynamic surface displacement transducer (IQI Model 501) by a non-contact method is presented. The transducer is designed for ultrasonic as well as acoustic emission measurements and, according to the manufacturer, its characteristic features include: a flat frequency response range which is from $50kHz$ to $1000kHz$ and a quality factor Q of less than unity. The characterization is based on the behavior of the transducer as a receiver and involves exciting the transducer directly by transient pulse input stress signals of quasi-electrostatic origin and observing its response in a digital storage oscilloscope. Theoretical models for studying the response of the transducer to pulse input stress signals and for generating pulse stress signals are presented. The characteristic features of the transducer which include the central frequency f_0, quality factor Q, and flat frequency response range are obtained by this non-contact characterization technique and they compare favorably with those obtained by a tone burst method which are also presented.

INTRODUCTION

In acoustic emission (AE) studies and ultrasonic testing (UT) of materials, a transducer may be defined as the element by which ultrasonic waves and pulses are introduced into or detected in materials. Its operation may be based on piezoelectric, piezomagnetic, thermal, electromagnetic or electrodynamic principles. Irrespective of the principle of operation, each transducer may be designated for one or more specific applications. It is often of interest to examine the behavior of the transducer so as to determine whether or not it meets its specifications.

This report examines the behavior of a novel transducer (IQI Model 501). The transducer is a product of Industrial Quality Incorporated (IQI) located in Gaithersburg, MD, $U.S.A$. It is designed for the detection of acoustic and ultrasonic waves. One characteristic feature of the transducer lies in its ability to detect short ultrasonic pulses, an ability which makes it useful for broadband ultrasonic measurements. The transducer is principally made of two components:

(1) a conically shaped piezoelement fabricated from lead zirconate-titanate (type: $PZT - 5A$) and

(2) a cylindrically shaped backing fabricated from brass.

The operational principle of the transducer is based on piezoelectricity. Piezoelectricity is a property of certain materials that manifests itself by the onset of electrical polarization (generation of bound charges of opposite polarity) when the material is subjected to mechanical stress and by the onset of mechanical deformation when it is subjected to an electrical field. In the first case, this behavior is called the direct piezoelectric effect and in the second, it is called the inverse piezoelectric effect.

Receiving transducers which are often referred to as receivers operate on the principle of the direct piezoelectric effect while transmitting transducers or transmitters operate on the inverse piezoelectric effect. Because many transducers are

designed to function as both receiver and transmitter, such transducers operate on both principles interchangeably. Transducer *IQI* Model 501 is designated to be a receiver and so its characteristic behavior is based on the direct piezoelectric effect.

Transducer characterization is a procedure which involves generating a known input signal and measuring the output signal of the transducer. The procedure sometimes involves mathematical modelling and analysis of the transducer, and a verification of the analytical model by experimental techniques.

The fundamental equations describing the piezoelectric effect were first documented about 50 years ago. A significant contribution to to the field was made by Mason [1] with the discovery that electromechanical behavior of piezoelectric crystals could be described by an equivalent electric circuit, with one electrical connection and two mechanical connections corresponding to the pair of electrodes on the two faces of the crystal. Several authors including Ryne [2], Smith and Awojobi [3], Kassof [4], and Sitting [5] have since employed Mason's model for studying many transducer phenomena. There have been several attempts by other authors [6-9] to develop electrical models to facilitate transducer analysis. Despite these attempts, the value of an equivalent circuit in understanding mechanical phenomena is quite limited.

Among the most significant work in predicting the electromechanical behavior of transducer system in that of Redwood [10, 11]. Some recent work including those of Williams and Doll [12] and Lee and Williams [13] have been based on Redwood's electromechanical model. Redwood's approach is adopted in this report.

A good literature review of experimental techniques for the characterization of transducers is presented by Sachse and Hsu [14]. The experimental methods of characterizing and/or calibrating a transducer involve the generation of step-function input signals to the face of the transducer and recording the response of the transducer in a storage oscilloscope. An ideal situation would be to generate a delta

function input to the transducer so that an impulse response of the transducer could be obtained directly; or to use sweeping continuous sine waves of varying frequencies to excite the transducer and to measure both the ratio of the magnitude and the difference of the phase angles of the input and output.

Conventionally, the generation of impulse function input signals can be achieved by one of several methods:

(1) breaking of glass capillary tube [15];

(2) breaking of pencil lead [16];

(3) dropping of steel ball impact [17];

(4) fracturing of silicon carbide particle [18];

(5) helium gas jet impact [19]; and

(6) laser pulse heating [20].

With each of these methods, the impulse-function input signal is transmitted to the transducer. The input signal is either applied directly on the face of the transducer by mechanical contact or through a propagation medium to which both the transmitting source and the transducer are coupled. In cases where the contact between the transducer and input signal is established through a medium, the true characteristics of the transducer are not easily determined unless the transfer function of the medium is known. By the transfer function of the medium is meant the exact response of the medium to the input signal. Therefore, the drawback of this method of coupling the input source to the transducer rests on the difficulties of determining the exact transfer function of the coupling medium. For this reason such methods as the breaking of a glass capillary tube and the fracturing of a pencil on the face of the transducer are favored in calibration of transducers because the impulse function time dependency is well defined and the absolute force can be measured independently with a static load cell.

While these techniques have the advantage of being simple and each produces

4

the characteristics of the transducer, they all suffer the disadvantage that the response signal obtained corresponds to a transducer coupled to load in air or another transducer which has a different mechanical impedance from the transducer itself.

The simplest medium would be no medium at all. This means that the input signal needs to be introduced directly onto the surface of the transducer and the transducer response be determined accordingly. Also an ideal impulse source needs to be obtained by electronic means which have the advantage of being very controllable and reproducible, rather than manually. Certainly, the repetition rate of electronically produced input signals is much faster than mechanical impacts which result from the breaking of a capillary tube or the fracturing of a pencil lead.

In this report, a non-contact technique is used to couple the transmitting source to the transducer. Pulse input stress signals of quasi-electrostatic origin are used for the excitation of the transducer. The pulse input stress signals are generated by quasi-electrostatic forces which are essentially the forces of attraction between a charged electric conductor and the surface of the piezoelement which is located at a specified distance from the electric conductor and carring electric charges of opposite polarity to those of the conductor. The electric charges on the conductor result from a transient electric current passing through the conductor while the charges on the surface of the piezoelement of the transducer are produced by quasi-electrostatic induction. So, the transducer, acting as a receiver and situated at a specified distance from the conductor, is excited by the transient stress signals. The detection of the transient stress signals is manifested by the voltage signal response of the transducer which is recorded in a digital storage oscilloscope. A duration of approximately 500 nanoseconds for the pulse input signals is chosen such that an approximate impulse response of the transducer is obtained.

Among other factors, the amplitude of the output voltage signals of the transducer may be affected by the conical shape of the piezoelement. Krautkramer and

Krautkramer [21] noted that the output voltage signals of any transducer are influenced by both the size and the geometry of the piezoelement. Detailed studies of the effect of the conical shape of the piezoelement on the output voltage signal of the transducer have been conducted theoretically in [22] and experimentally in [23].

As a check on the results obtained from the non-contact characterization technique, the results are compared wth those obtained from the tone burst method which is a common characterization technique. The results from the two techniques compare favorably. The tone burst results are appended to this report.

DESCRIPTION OF DYNAMIC SURFACE DISPLACEMENT TRANSDUCER
(IQI MODEL 501)

The dynamic surface displacement transducer is a product of Industrial Quality Incorporated which is located in Gaithersburg, *MD*, *U.S.A.*. The transducer is designated as *IQI* Model 501 and is described by the manufacturer as having the following characteristic features:

(a) flat frequency response sensitivity range is from 50 kHz to 1000 kHz, which represents broadband characteristics;

(b) displacement sensitivity h is equal to 2×10^8 volt/m; and

(c) mounted quality factor Q is less than 1.

The complete unit of the transducer is made of two major parts, namely,

(a) the transducer unit which is shielded circumferentially by plastic, and

(b) the electronic unit.

Schematics of the transducer without and with the plastic (plexiglass) shield, are shown in Figs. 1 and 2, respectively. The transducer unit consists of two components:

(a) a conically shaped piezoelement which is fabricated from lead zirconate-titanate (type $PZT - 5A$); and

(b) a cylindrically shaped backing fabricated from brass.

The truncated end of the piezoelement has a diameter (contact size) of about 59×10^{-3} in (1.5 mm), a thickness (length) of about 98×10^{-3} in (2.50 mm), and a base diameter of about 177×10^{-3} (4.50 mm). The included angle of the piezoelement is 80°. It is attached by heat-cured epoxy resin to the backing of 0.75 in (19.50 mm) in diameter and 1.0 in (25.40 mm) in length. On the two opposite faces of the piezoelement there are evaporated silver films which form the electrodes of the transducer.

During use, one electrode of the piezoelement is electrically connected to the electronic unit through an electric lead which is connected through the backing while the other is placed on a metallic medium which completes the electric circuit. Electrically, the backing acts as the non-grounded electrode for signal detection. The lower smaller electrode becomes the grounded mounting surface. Any stress signal incident on the piezoelement tip excites the transducer and the resulting voltage signal of the transducer is the potential difference between the backing and the tip of the piezoelement.

The electronic unit consists of an amplifier (gain: 1 dB) which is mounted on the inside face of a hollow cylinder fabricated from aluminum and a 9-volt battery which is mounted beside the amplifier. A schematic of the electronic circuit is shown in Fig. 3. Through a BNC jack attached on the outside face of the hollow cylinder (container), the electronic circuit is hooked up to other electronic units such as oscilloscope and amplifiers. The container is covered by cap that is similarly fabricated from aluminum.

Figs. 4a and 4b show schematics of the cap and the container, respectively.

Advantages of the Design of the Transducer

Unlike conventional pulse/echo piezoelectric transducers which are made of a shoe, piezoelement, backing, casing and connector as shown in Fig. 5, design of transducer IQI is simple because the transducer unit consists of only a piezoelement and the backing. One other drawback of the conventional design is that the transducer unit together with the case, connector and lead form a complex structure which is subject to multiple resonances. Also, interference effects associated with various dimensions such as the shoe thickness can cause variations in transducer response. In the present design, the large radial and axial size of the backing eliminates any such thickness resonance and interference effects. Also, the weight ($2.83N$) of the transducer unit provides a coupling pressure of approximately $4.00 \times 10^5 N/m^2$

(58 psi) which exceeds the saturation pressure of $2.5 \times 10^5 N/m^2$ (36psi) which is defined as the minimum transducer-specimen interface pressure which results in the maximum amplitude of the output signal, all other parameters being held constant [24]. No intermediate liquid such as $AET \quad SC-6$ is needed to couple the transducer to media whose ultrasonic or acoustic emission measurements are being sought.

By virtue of the conical shape of the piezolement of the transducer, the surface area of the transducer is kept small, a feature which makes the transducer an approximation to a point receiver. Specifically, the 1.5mm (smaller) diameter of the piezoelement of the transducer is small compare with the wavelengths which vary from 4.35mm to 87.00mm over the transducer's frequency response range which is from $50kHz$ to $1000kHz$. This small transducer area provides a high sensitivity. Also, its broadband characteristics make it very useful for AE measurements because AE signals are complex signals which represent broadband energy sources.

Applications of the Transducer

Accordingly to the manufacturer, the transducer can be used for the following applications:

(a) AE monitoring of structural components;

(b) comparison calibration (as secondary standard) for AE or ultrasonic transducers;

(c) calibration of complete AE measurement system;

(d) high fidelity ultrasonic detection in solids; and

(e) calibration of complete ultrasonic spectroscopy systems.

ANALYSIS OF TRANSDUCER RESPONSE TO
PULSE INPUT SIGNALS

Here, the behavior of the transducer when subjected to a pulse input stress is analyzed. The mechanism by which the pulse input stress is detected by the transducer is also presented.

A good starting point is to derive and solve the equation of motion of the piezoelement when it is subjected to longitudinal stress. This involves the examination of one dimensional plane wave propagation in the piezoelement. Fig. 6 illustrates the conically shaped piezoelement supporting one dimensional wave propagation. The derivation of the equation of motion of the piezoelement was presented in [22] and the equation can be reproduced as

$$\frac{\partial}{\partial x}\left[\left(A(x)\frac{\partial u(x,t)}{\partial x}\right)\right] = \frac{1}{c_p{}^2}A(x)\frac{\partial^2 u(x,t)}{\partial t^2} \quad , \tag{1}$$

where $A(x)$ [in^2] is the variable cross sectional area, c_p [in/sec] is the longitudinal wave speed in the piezoelement, and $u(x,t)$ [in] is the displacement which is a function of both space x and time t.

With the use of the *WKBJ* (Wentzel-Kramers-Brillouin-Jeffreys) approximate solution technique, the effect of the variable cross section of the piezoelement on the amplitude of the longitudinal wave as it propagates from one location of the piezoelement to another was examined in detail in [22]. Specifically, it was shown that the ratio of the amplitudes of the propagating wave at the locations $x = 0$ and $x = L$ are related to the ratio of the radii of the piezoelement at those respective locations by

$$\frac{a(x_L)}{a(x_0)} = \frac{r(x_0)}{r(x_L)} \tag{2}$$

where $a(x_0)$ and $a(x_L)$ represent the amplitudes of the wave and $r(x_0)$ and $r(x_L)$ represent the radii at $x = 0$ and $x = L$, respectively.

Since the variable cross section of the piezoelement does not affect the time-behavior of the wave, it seems appropriate to set aside its effect on the propagating wave, to solve the wave equation and to include the effects of the variable cross section later. In other words, for the time being assume that $A(x)$ is constant. Also, in solving the wave equation, the effect of piezoelectricity in the rod which is neglected at first is included later.

If $A(x)$ is assumed to be constant, then eqn.(1) becomes

$$\frac{\partial^2 u(x,t)}{\partial x^2} = \frac{1}{c_p{}^2}\frac{\partial^2 u(x,t)}{\partial t^2} \quad , \tag{3}$$

where the argument "(x,t)" of u will be dropped subsequently.

Because transient performance of the transducer is of interest here, an operational calculus technique or the so called Laplace transform may be utilized to solve eqn.(3). Redwood [10] used this method for presenting a solution of eqn (3). The Laplace transform is defined as [25]

$$\mathcal{L}f(t) = f'(p) = \int_0^\infty exp(-pt)f(t)dt \quad , \tag{4}$$

where $\mathcal{L}$ is the symbol for Laplace transform, $f'(p)$ is the Laplace transform of the function $f(t)$, and p is the Laplace transform variable.

Throughout this analysis, the Laplace transform of quantities will be referred to by the names of the quantities themselves: for instance, u' will be referred to as a displacement. It will be understood from the superscript $'$ that it is actually the Laplace transform of the variable that is being considered, rather than the variable itself.

If the value of the function $f(t)$ is zero at $t = 0$, it may be shown that [25]

$$\left\{\frac{df(t)}{dt}\right\} = pf'(p) \quad , \tag{5}$$

and consequently that

$$\left\{\frac{d^2 f(t)}{dt^2}\right\} = p^2 f'(p) \quad , \tag{6}$$

11

if also the value of $df(t)/dt$ is zero at $t = 0$.

Applying the Laplace transform operation to eqn.(3) yields the transformed one dimensional plane wave equation

$$\frac{\partial^2 u'}{\partial x^2} = \frac{p^2}{c_p{}^2} u' \quad , \tag{7}$$

where u' is the Laplace transform of $u(t)$.

Eqn.(7) in a linear second-order partial differential equation with constant coefficients and its solution can be written as the sum of two exponentials

$$u' = A \, exp\left(-\frac{px}{c_p}\right) + B \, exp\left(\frac{px}{c_p}\right) \quad . \tag{8}$$

The first term of eqn.(8) represents a wave propagating in the positive x-direction and the second term represents a wave propagating in the negative x-direction. A and B are amplitude factors that are determined from the boundary conditions.

The relationship between stress and displacement in a nonpiezoelectric material is given by Hooke's Law as

$$\sigma' = E \frac{\partial u'}{\partial x} \tag{9}$$

where σ is the stress in x-direction and E is the modulus of elasticity.

Substituting for the quantity $\partial u'/\partial x$ from eqn.(8) into eqn.(9) gives

$$\sigma' = E \frac{p}{c_p} \left[-A \, exp\left(-\frac{px}{c_p}\right) + B \, exp\left(\frac{px}{c_p}\right) \right] \quad . \tag{10}$$

Recall that E is related to the product of the density and the square of the longitudinal wave speed by

$$E = \rho c_p{}^2 \quad . \tag{11}$$

Then eqn.(10) may be rewritten as

$$\sigma' = \rho c_p p \left[-A \, exp\left(-\frac{px}{c_p}\right) + B \, exp\left(\frac{px}{c_p}\right) \right] \quad . \tag{12}$$

12

The quantity ρc_p is the ratio of the stress to the particle velocity in the material, and it is known as the characterstic impedance and is denoted here by Z_p. Thus,

$$Z_p = \rho c_p \quad , \tag{13}$$

and eqn.(12) becomes

$$\sigma' = Z_p p \left[-A\,exp\left(-\frac{px}{c_p}\right) + B\,exp\left(\frac{px}{c_p}\right) \right] \quad . \tag{14}$$

This is the equation for stress in the x-direction of a nonpiezoelectric material which satisfies the one dimensional plane longitudinal wave equation.

In order to incorporate the effects of piezoelectricity into the solution of the wave equation, recall that Hooke's Law for piezoelectric materials requires that

$$\sigma' = E\frac{\partial u'}{\partial x} - hD \quad . \tag{15}$$

This equation shows that the presence of an electric flux D [coul/in^2] in the x-direction produces a so called "piezoelectric stress" hD [lb/in^2], where h [volt/in] is the piezoelectric constant of the material.

To obtain a relationship between stress and electric flux in the piezoelement, substitute eqn.(14) into the Laplace transform of eqn.(15)

$$\sigma' + hD = Z_p p \left[-A\,exp\left(-\frac{px}{c_p}\right) + B\,exp\left(\frac{px}{c_p}\right) \right] \quad . \tag{16}$$

The flux density D in the transducer is a constant function of x as shown in [22]. The presence of the stress produces an electric charge of quantity Q' and the flux density is related to this charge by Gauss's Law. Thus,

$$D = \frac{Q'}{A_p} \quad , \tag{17}$$

where A_p is the surface area of the piezoelement (see Fig. 7).

13

Substituting eqn.(17) into eqn.(16) gives the following general equation for stress in the piezoelement:

$$\sigma' + \frac{hQ'}{A_p} = Z_p p \left[-A\, exp\left(-\frac{px}{c_p} \right) + B\, exp\left(\frac{px}{c_p} \right) \right] \quad . \qquad (18)$$

To determine the voltage across the piezoelement, the following equation must be used [10]:

$$\frac{\partial \phi'(x,p)}{\partial x} = h\frac{\partial u'}{\partial x} + \frac{D}{\varepsilon} \quad , \qquad (19)$$

where $\phi'(x,p)$ is the local potential in the piezoelement and ε [farads/in] is the absolute permittivity of the piezoelectric material.

To solve for V' the total voltage across the piezoelement, eqn.(19) must be integrated along the x-axis from O to L (see Fig. 7).

$$V' = \int_0^L \frac{\partial \phi'(x,p)}{\partial x}dx = -hu' \Big|_{x=0}^{x=L} + \frac{DL}{\varepsilon} \quad . \qquad (20)$$

The third term in eqn.(20) can be simplified by realizing that Gauss's Law can again be used to determine the capacitance C_0 of the unstressed piezoelement as

$$C_0 = \frac{\varepsilon A_p}{L} \quad . \qquad (21)$$

Substituting eqns.(21) and (17) into eqn.(20) gives the transducer voltage in terms of charge

$$V' = -hu' \Big|_{x=0}^{x=L} + \frac{Q'}{C_0} \quad . \qquad (22)$$

This is the equation relating the quantities of displacement, voltage and charge in a piezoelectric transducer.

In order to relate the electric response of the transducer to the pulse input stress, consider the incident pulse input stress on the piezoelement shown in Fig. 7. A_1 is the displacement associated with the incident wave in air, and B_1 and A are the amplitudes of the reflected and transmitted displacement waves, respectively, which

are produced when wave A_1 strikes the air-piezoelement interface. The boundary conditions at the interface at $x=0$ are

$$u_1' \Big|_{x=0} = u' \Big|_{x=0} \tag{23}$$

and

$$\sigma_1' \Big|_{x=0} = \sigma' \Big|_{x=0} \tag{24}$$

where the quantities without subscripts refer to the piezoelement and those subscripted with 1 refer to the air.

Substituting eqn.(8) into eqn.(23), and eqn.(18) into eqn.(24), the boundary conditions become

$$A_1 + B_1 = A + B \quad . \tag{25}$$

$$pZ_a(-A_1 + B_1) = pZ_p(-A + B) - \frac{hQ'}{A_p} \tag{26}$$

If the analysis is restricted to values of times less than that required for wave A to reach the piezoelement-backing interface, wave B may be ignored. So, eqns.(25) and (26) become

$$A_1 + B_1 = A \tag{27}$$

and

$$pZ_a(A_1 + B_1) = -pZ_pA - \frac{hQ'}{A_p} \tag{28}$$

Solving eqn.(27) for B_1 and substituting this value into eqn.(28) give

$$-2A_1\,pZ_a + AZ_a = -AZ_p - \frac{hQ'}{A_p} \quad . \tag{29}$$

Eqn.(29) relates the mechanical quantities A_1 and A to the charge Q' on the piezoelement. If a resistance R is connected across the piezoelement, the voltage V' may be expressed as

$$V' = I'R = -pQ'R \quad , \tag{30}$$

15

where I' represents the current in amperes through the resistance R in ohms, Q' is the charge on the piezoelement in coulombs, and p is the Laplace transform variable. Substituting eqn.(30) into eqn.(29) and collecting terms yield

$$Ap(Z_a + Z_p) = \frac{hV'}{prA_p} + 2A_1PZ_a \quad , \tag{31}$$

and solving for A yields

$$A = \left(\frac{hV'}{pRA_p} + 2pZ_aA_1 \right) [p(Z_a + Z_p)]^{-1} \quad . \tag{32}$$

This equation relates the amplitude of the displacement wave A and the voltage V' produced in the piezoelement to the amplitude of the incident displacement A_1.

Eqn.(22), reproduced here as

$$V' = hu' \Big|_{x=0}^{x=L} + \frac{Q'}{C_0} \quad . \tag{33}$$

gives the voltage across the piezoelement in terms of the displacement.

Substituting eqn.(8) into the first term of eqn.(33), and eqn.(30) into the second term of eqn.(33) gives

$$V' = h \left[A\,exp \left(-\frac{pL_p}{c_p} - 1 \right) \right] - \frac{V'}{pRC_0} \quad . \tag{34}$$

Note that L_p/c_p is the time required for a wave to pass from the air-piezoelement interface to the piezoelement-backing interface. Denoting this time by t_p, eqn.(34) becomes

$$V' = -hA\,[exp(-pt_p) - 1] - \frac{V'}{pRC_0} \quad , \tag{35}$$

and substituting for A from eqn.(32) yields

$$V' - \frac{h}{p(Z_a + Z_p)} \left[\frac{hV'}{pRA_p} + 2pZ_1A_1 \right] [exp(-pt_p) - 1] - \frac{V'}{pRC_0} \quad . \tag{36}$$

Solving for V' gives

$$V' = 2hA_1 \left[\left(\frac{Z_a}{Z_a + Z_p} \right) \left(\frac{p^2\,[1 - exp(-pt_p)]}{p^2 + \frac{p}{RC_0} - \frac{h^2[1-exp(-pt_p)]}{RA_p(Z_a+Z_p)}} \right) \right] \quad . \tag{37}$$

16

The quantity V' is the voltage [volt] generated across the piezoelement when a displacement wave of amplitude A_1 impinges upon it from an adjacent medium of impedance Z_a [lb/in-sec]. The quantity h [volt/in] is the deformation constant of the piezoelement, R [ohms] and C_0 [farads] are the resistance and capacitance of the piezoelement, respectively, and A_p [in^2] and Z_p [lb/in-sec] are the surface size area and the impedance of the piezoelement, respectively.

In order to relate the voltage to the incident stress, eqn.(37) needs to be cast in terms of the stress. If σ_i is the amplitude of the incident pulse input stress, its Laplace transform can be expresed as [25]

$$\sigma' = \mathcal{L}\left(\sigma(t)\right) = \frac{\sigma_i}{p}\left[1 - exp(-pt_d)\right] \quad , \qquad (38)$$

where the time-domain function of the stress is given by

$$\sigma(t) = \begin{cases} \sigma_i = constant & for \ 0 < t < t_d \\ 0 & for \ t < 0, \ t_d < t \end{cases} \quad , \qquad (39)$$

where t_d is the duration of the pulse (see Fig. 8). Note that the pulse function $\sigma(t)$ may be considered as a step function of height σ_i which begins at $t = 0$ and which is superimposed by a negative step function of height σ_i beginning at $t = t_d$, namely,

$$\sigma(t) = \sigma_i(t) - \sigma_i(t - t_d) \quad . \qquad (40)$$

At $x = 0$, the Laplace transform of the incident stress is equal to the left-hand side of eqn.(28). Thus,

$$\sigma' = -pZ_aA_1 \quad , \qquad (41)$$

when the initial displacement condition u(x,0) is zero. Combining eqns.(38) and (41) gives

$$\frac{\sigma_i}{p}\left[1 - exp(-pt_d)\right] = pZ_aA_1 \quad . \qquad (42)$$

Solving for A_1 in terms of σ_i gives

$$A_1 = -\frac{\sigma_i}{p^2Z_a}\left(1 - exp(pt_d)\right) \quad . \qquad (43)$$

Substituting this value for A_1 into eqn.(37) results in

$$V' = -\frac{2h\sigma_i\,[1 - exp(-pt_d)]}{Z_a + Z_p} \left\{ \frac{1 - exp(-pt_p)}{p^2 + \frac{p}{RC_0} - \frac{h^2[1 - exp(-pt_p)]}{RA_p(Z_a + Z_p)}} \right\} \quad , \qquad (44)$$

which gives V' in terms of the amplitude σ_i of a pulse function of stress.

Examination of eqn.(44) shows that the factor $exp(-pt_p)$ appears twice. This factor represents a time delay [11] equal to t_p, so that the terms by which it is multiplied do not show up at the same time as the rest of the terms in eqn.(44). Restricting the analysis to values of time less than the time t_p, these delay terms must then be struck from the equation. So, taking only those terms which show up immediately, the expression for V' becomes

$$V' = -\frac{2h\sigma_i}{Z_a + Z_p} [1 - exp(-pt_d)] \left[p^2 + \frac{p}{RC_0} - \frac{h^2}{RA_p(Z_a + Z_p)} \right]^{-1} \quad . \qquad (45)$$

The denominator of eqn.(45) is quadratic in p and may be written as the product $(p + \tau_1)(p + \tau_2)$, where

$$\tau_1,\tau_2 = -\frac{1}{2RC_0} \pm \left[\left(\frac{1}{2RC_0} \right)^2 + \left(\frac{h^2}{RA_p(Z_a + Z_p)} \right) \right]^{1/2} \quad . \qquad (46)$$

Also, the term "$exp(-pt_d)$" can be expressed as [25]

$$exp(-pt_d) = 1 - \frac{pt_d}{1!} + \frac{(pt_d)^2}{2!} - \cdots \quad . \qquad (47)$$

Substituting eqn.(47) into eqn.(45) and neglecting higher order terms in p give

$$V' = -\frac{2h\sigma_i\,t_d}{Z_a + Z_p} \left[\frac{p}{(p + \tau_1)(p + \tau_2)} \right] \quad . \qquad (48)$$

The inverse Laplace transform of eqn.(48) in terms of the time constants τ_1 and τ_2 can be written as [11]

$$V(t) = -\frac{2h\sigma_i\,t_d}{(Z_a + Z_p)} \left[\frac{(\tau_2)exp(-t\tau_2) - (\tau_1)exp(-t\tau_1)}{\tau_2 - \tau_1} \right] \quad . \qquad (49)$$

This equation gives the time-dependent output voltage which is produced across the piezoelement by a pulse input stress of amplitude σ_i. The time t_d is the duration of the pulse.

DETECTION MECHANISM OF INPUT STRESS PULSE

Understanding the detection mechanism of the input stress pulse is important in analyzing the response of the transducer. In order to facilitate the analysis, consider an input stress pulse signal incident on the transducer. A schematic of the input stress pulse signal is shown in Fig. 9a while the transducer is schematically shown in Fig. 9b as a two-layer material of lengths L_p and L_b representing the piezoelement and the backing, respectively. The quantities Z_p and c_p, and Z_b and c_b in Fig. 9b represent the acoustic parameters of the piezoelement and the backing, respectively. The acoustic parameters Z_a and c_a of air are also indicated in Fig. 9b. Also, consider the schematic of the transducer's response as represented in Fig. 9c.

When the stress pulse becomes incident on the piezoelement, there results an average strain ϵ in the piezoelement and a steady potential difference across the piezoelement.The average strain ϵ is given by

$$\epsilon = \frac{\Delta L_p}{L_p} \tag{50}$$

where ΔL_p is the average change in length of the piezoelement and L_p is the length of the piezoelement. The potential difference across the piezoelement or the voltage signal produced can be detected if a resistor is connected across the piezoelement when the stress is removed. The voltage signal is proportional to the average strain and it is also the first voltage signal of the transducer with an amplitude say unity.

After a time

$$t_p = \frac{L_p}{c_p} \tag{51}$$

where c_p is the wave speed in the piezoelement, the stress signal reaches the opposite face of the piezoelement. When the stress signal arrives on this face a second voltage signal across the piezoelement is produced and it can be detected in this manner as the first.

19

It is important to mention that when the stress signal becomes incident on the air-piezoelement interface, a part of the stress signal is reflected and the other part is transmittted. The amplitude of the reflected signal is given by

$$\sigma_R = R_0 \sigma_i \quad , \tag{52}$$

where R_0 is the reflection coefficient at the air-piezoelement interface which is defined by

$$R_0 = \frac{Z_p - Z_a}{Z_p + Z_a} \quad , \tag{53}$$

where Z_p and Z_a are the characteristic impedances of the piezoelement and the air, respectively. The quantity σ_i is the amplitude of the incident stress wave signal. Also, the part of the stress which is transmitted into the piezoelement is given by

$$\sigma_T = T_0 \sigma_i \tag{54}$$

where

$$T_0 = \frac{2Z_p}{Z_p + Z_a} \tag{55}$$

is the transmission coefficient at the air-piezoelement interface.

At the location $x = L_p$, the reflection and transmission coefficients are given by

$$R_x = \frac{Z_b - Z_p}{Z_b + Z_p} \tag{56}$$

and

$$T_x = \frac{2Z_b}{Z_b + Z_p} \quad , \tag{57}$$

where Z_b is the characteristic impedance of the backing.

The reflected stress signal returns to $x = 0$, where it is reflected with the reflection coefficient R_0. This stress signal produces the third voltage signal at $t = 2L_p/c_p$. Other electrical signals may be produced by later reflections as shown in Fig. 9c. Since R_0 and R_x may have values between $+1$ and -1, many combinations

of polarities may be found in the reflections. It should be noted that if the duration of the stress pulse is longer than L_p/c_p, then overlapping of electrical signals may occur. It should also be noted that L_b is assumed sufficiently large so that during the period of observation the stress signals transmitted through the piezoelement-backing interface do not return to the interface. Therefore, the observed output electrical signals from the transducer exclude the contributions from such signals. If the impedance of the piezoelement is in excellent match with that of the backing then only the first two voltage signals are produced.

So far, the discussion of the detection mechanism excluded the effect of the variable cross section of the piezoelement on the amplitude of the stress signal as it travels from one face of the piezoelement to the other; and hence on the amplitude of the electrical signal produced by the transducer. The effect of the variable cross section can be included by using the $WKBJ$ approxmation [22] on the amplitude of the output voltage if eqn.(49) is modified as

$$V(t) = -\frac{2h\sigma_i t_d}{Z_a + Z_p} \cdot \frac{r(x_1)}{r(x_2)} \left[\frac{(\tau_2)exp(-t\tau_2) - (\tau_1)exp(-t\tau_1)}{\tau_2 - \tau_1} \right] \quad . \quad (58)$$

where $r(x_1)$ and $r(x_2)$ are the cross sectional radii of the truncated end and the base of the piezoelement, respectively.

Eqn. (58) suggests that the effect of the tapering of the piezoelement is to reduce the voltage amplitude. Also, in the experimental study of wave propagation in conically shaped isotropic rods [23], the authors noted that the average deviation due geometrical spreading of a propagating wave through the piezoelement is 25% when the transducer is operated within a frequency range of $200kHz$ to $1000kHz$.

Before concluding this discussion, it is important to mention that in practice the voltage signals are recorded on an oscilloscope which is electrically connected to the transducer through two electrodes deposited on the two faces of the piezoelement. So, by modelling the piezoelement and backing as two capacitors connected in series, one can say that the voltage signal observed on the oscilloscope is the potential

difference across the two elements. A schematic of the electrical circuit representing this model is shown in Fig. 10. The upper capacitor, denoted by C_b represents the backing and lower capacitor C_p represents the piezoelement.

The potential difference V_p across C_p is given by

$$V_p = \frac{Q_p}{C_p} \quad , \tag{59}$$

and that across C_b is given by

$$V_b = \frac{Q_b}{C_b} \tag{60}$$

where Q_p is the quantity of charge produced by the piezoelement due to the stress signal and Q_b is the quantity of charge induced on the backing. But the potential difference across the two serially connected capacitors is the sum of these potential differences. Therefore, the potential difference across the two elements is

$$V = \frac{Q_p}{C_p} + \frac{Q_b}{C_b} \quad . \tag{61}$$

If the piezoelement is electrically matched, then C_p is equal to C_b and Q_p is equal to Q_b. In that case the total potential difference becomes

$$V = \frac{2Q_p}{C_p} \quad . \tag{62}$$

Also, if the oscilloscope is electrically matched to the transducer, then the voltage signal observed on the oscilloscope is exactly that predicted by eqn.(62). This is usually the goal in practice.

GENERATION OF INPUT STRESS PULSE SIGNALS BY
QUASI-ELECTROSTATIC FORCES

Here the method for generating input stress pulse signals to the transducer is presented. The source for generating the input stress signals to the transducer is modelled as a rectangular electric conductor C which is supporting an electric current I. The surface area of the piezoelement of the transducer is modelled as a conical surface which is located at a perpendicular distance z from the conductor. A schematic of this arrangement is shown in Fig. 11.

When electric current passes through the conductor, electric charges quantity of say $-q$ are produced on the surface of the conductor. At the same instant electric charges of opposite polarity of quantity $+q$ are produced on the surface of the piezoelement due to quasi-electrostatic induction. Due to the existence of these electric charges of opposite polarity on the surfaces of the conductor and the piezoelement, there exists a quasi-electrosatic force of attraction between them. The magnitude of the quasi-electrostatic force acting on the piezoelement can be calculated if the magnitude of the electric field at surface of the piezoelement is known.

For simplicity, assume that the total charge on the piezoelement is concentrated at its center P. So, the magnitude of the electric field at this point determines the total electric field on the entire surface of the piezoelement.

In order to calculate magnitude of the electric field, consider that the point P is located at a distance z along the z-axis from a rectangular electric conductor of dimensions l_x and l_y supporting an electric current of magnitude I. The xyz-coordinate system lies at its center. A schematic of the conductor and the geometric parameters of the point are shown in Fig. 12. The presence of of the electric current in the conductor produces an electric field $\mathbf{E}$. For clarity, the electric field $\mathbf{E}$ is sketched separately in Fig. 12c.

The electric field $d\mathbf{E}$ at a point P set up by a charge element $\gamma\,dx\,dy$ located at point A on the xy plane can be written from Gauss's Law as [26]

$$d\mathbf{E} = k\frac{\hat{\mathbf{s}}}{s^2}\gamma\,dx\,dy \quad , \tag{64}$$

where $\hat{\mathbf{s}}$ [in] is the unit vector pointing from A to P. The point P lies at a distance

$$s = \sqrt{x^2 + y^2 + z^2} \tag{65}$$

from the charge element at A. The quantity γ [coul/m^2] is the surface charge density of the conducting plate, and k [N-m/coul^2] is the coulomb constant which is defined as

$$k = \frac{1}{4\pi\varepsilon_0} \quad , \tag{66}$$

where ε_0 is the permittivity of free space. Note that all letters in boldface are vector quantities. The location of the charge element is known as the *source point*, while the location at which the electric field is observed is known as the *field point*.

The resultant electric field $\mathbf{E}$ at P is the vector sum of the contributions of electric fields from all the charge elements. Therefore,

$$\mathbf{E} = \int_{-l_x/2}^{+l_x/2} dx \int_{-l_y/2}^{+l_y/2} dy\, k\gamma\frac{\mathbf{s}}{s^2} \quad . \tag{67}$$

By symmetry arguments, the x- and y-components are zero because of the following reason. For every charge element $\gamma\,dx\,dy$ at location (x,y), there is a corresponding charge element at location $(-x,-y)$. The components dE_x and dE_y set up by one of these charge elements are equal in magnitude but opposite in sign to those set up by the corresponding charge element and therefore, they cancel each other. So, the only nonzero component of the electric field $\mathbf{E}$ is E_z.

The z-component of the electric field can be written from eqn.(67) as

$$E = E_z = 4kz\gamma \int_0^{l_x/2} dx \int_0^{+l_y/2} dy\, \left(x^2 + y^2 + z^2\right)^{-3/2} \quad . \tag{68}$$

24

The factor 4 in eqn.(68) results from the fact that $\int_{-a}^{a} \int_{-b}^{b} = 4 \int_{0}^{a} \int_{0}^{b}$.

Integration of eq.(68) can be obtained in two major steps:

(a) The y-integration: Integration with respect to y requires the following substitutions:

$$y = \sqrt{x^2 + z^2} \tan u \quad , \tag{69a}$$

$$dy = \sqrt{x^2 + z^2} \sec^2 u \tag{69b}$$

where u is the new variable. The new limits of integration u_1 and u_2 are determined as follows:

$$y = 0 \Rightarrow u_1 = 0 \quad , \tag{69c}$$

and

$$y = l_y/2 \Rightarrow u_2 = \tan^{-1} \frac{l_y/2}{\sqrt{x^2 + z^2}} \quad . \tag{69d}$$

Therefore,

$$\int_0^{l_y/2} dy \, (x^2 + y^2 + z^2)^{-3/2} = \int_0^{u_2} du \, \left(\sqrt{x^2 + z^2} \right) \left[(x^2 + z^2) \sec^2 u \right]^{-3/2} \quad . \tag{69e}$$

Integrating the right-hand side of eqn.(69e) results in

$$\int_0^{l_y/2} dy \, (x^2 + y^2 + z^2)^{-3/2} = \frac{1}{x^2 + z^2} \frac{l_y/2}{\sqrt{x^2 + (l_y/2)^2 + z^2}} \quad . \tag{69f}$$

(b) The x-integration: Integration of eqn.(69f) with respect to x requires the following substitutions:

$$\frac{1}{(x^2 + z^2)} = \frac{1}{i2z} \left(\frac{1}{x + iz} - \frac{1}{x - iz} \right) \tag{70a}$$

$$v_1 = x + iz \quad , \tag{70b}$$

$$v_2 = x - iz \quad . \tag{70c}$$

The limits of integration are

$$x = 0 \Rightarrow v_1 = iz \quad and \quad v_2 = -iz \quad , \tag{70d}$$

and

$$x = l_x/2 \Rightarrow v_1 = (l_x/2) + iz \quad and \quad v_2 = (l_x/2) - iz \quad , \qquad (70e)$$

Therefore, the integral of the right-hand side of eqn.(69f) becomes

$$\int_0^{l_x/2} dx \frac{1}{x^2 + z^2} \frac{l_y/2}{\sqrt{x^2 + z^2 + (l_y/2)^2}} = \frac{i}{2z} \left[\int_{iz}^{(l_x/2)+iz} dv_1 \frac{1}{v_1} \frac{l_y/2}{\sqrt{(v_1 - iz)^2 + z^2 + (l_y/2)^2}} \right.$$
$$\left. + \int_{-iz}^{(l_x/2)-iz} dv_2 \frac{1}{v_2} \frac{l_y/2}{\sqrt{(v_2 + iz)^2 + z^2 + (l_y/2)^2}} \right]$$

$$(70f)$$

Integrating the right-hand side of eqn.(67f) results in

$$\int_0^{l_x/2} dx \frac{1}{x^2 + z^2} \frac{l_y/2}{\sqrt{(x^2 + z^2 + (l_y/2)^2}} = \frac{1}{z} \left[\frac{\pi}{2} - tan^{-1} \left(\frac{2z}{l_x} \right) - tan^{-1} \left(\frac{z l_x}{A} \right) \right] \quad .$$

$$(70g)$$

where

$$A = 2 \left[z^2 + (l_y/2)^2 + \frac{l_y}{2} \sqrt{z^2 + (l_x/2)^2 + (l_y/2)^2} \right] \quad . \qquad (70h)$$

Combining eqns.(70g) and (68) gives

$$E = 2k\pi\gamma \left[1 - \frac{2}{\pi} tan^{-1} \left(\frac{2z}{l_x} \right) - \frac{2}{\pi} tan^{-1} \left(\frac{z l_x}{A} \right) \right] \quad . \qquad (71)$$

Notice that as z tends to zero, E approaches $2k\pi\gamma$, which is the electric field due to an infinite plane conductor.

By definition, γ is given by

$$\gamma = \frac{q}{A_c} \quad , \qquad (72)$$

where q is the total quantity of electric charge on the surface of the conductor and A_c is the surface area of the conductor. So, combining eqns. (71) and (72) gives

$$E = 2k\pi \frac{q}{A_c} \left[1 - \frac{2}{\pi} tan^{-1} \left(\frac{2z}{l_x} \right) - \frac{2}{\pi} tan^{-1} \left(\frac{z l_x}{A} \right) \right] \quad . \qquad (73)$$

The magnitude of the quasi-electrostatic force F and hence the force of attraction between the conductor and the piezoelement is given by [26]

$$F = -qE \qquad (74)$$

26

where q is the magnitude of the total quantity of the electric charge on the surface of the piezoelement and negative sign indicates attraction. The quantity q is related to the electric current by [26]

$$q = It \qquad (75)$$

where I is the magnitude of the electric current and t is the time it takes to switch on electric current to the conductor.

If the electric current is transient, then the electric charge is also transient and so are the electric field and quasi-electrostatic force. Therefore, eqn. (74) can be rewritten as

$$F(t) = -q(t)E(t) \qquad (76)$$

As a result of the quasi-elecrostatic force transient stress signal is generated on the surface of the piezoelement of the transducer. The magnitude of the stress signal which is denoted by $\sigma_i(t)$ is the ratio of the quasi-electrostatic force and the surface area of the piezoelement. Thus,

$$\sigma_i(t) = \frac{F(t)}{A_p} \qquad (77)$$

where A_p is the surface area of the piezoelement of the transducer.

Combining eqns. (73) through (77) gives

$$\sigma_i(t) = -\frac{2k\pi I^2(t)\, t^2}{A_c A_p} \left[1 - \frac{2}{\pi} tan^{-1} \left(\frac{2z}{l_x} \right) - \frac{2}{\pi} tan^{-1} \left(\frac{z l_x}{A} \right) \right] \qquad (78)$$

Eqn.(73) gives the final expression of the transient stress signal due to quasi-electrostatic force.

Also, there is another quasi-electrostatic stress which results from electromagnetic radiation when a transient electric current is allowed to pass through the condutor. The contribution from electromagnetic radiation can be calculated if the magnetic field at point P is known.

27

The magnetic field **dB** at P set up by a current element $K\,dx\,dy$ located at point A can be written from the Biot-Savart Law as [26]

$$\mathbf{dB} = \frac{\mu_0}{4\pi}\frac{\hat{y}\times\hat{s}}{s^2}K\,dx\,dy \quad , \tag{79}$$

where μ_0 [N/amperes] is the permeability constant in free space and K [amps/m] is the surface current density. The unit vector $\hat{y}$ points in the positive y-direction. A schematic of the magnetic field is shown in Fig. 12d.

By symmetry, only the x-component of the magnetic field survives for field points on the z-axis. So,

$$B = B_x = 4\frac{\mu_0 K z}{4\pi}\int_0^{l_x/2}dx\int_0^{l_y/2}dy\;(x^2+y^2+z^2)^{-3/2} \tag{80}$$

Note that the integrals in eqn.(80) are identical to those of eqn.(67). After simplification, eqn.(80) becomes

$$B = \frac{K\mu_0}{2}\left[1 - \frac{2}{\pi}tan^{-1}\left(\frac{2z}{l_x}\right) - \frac{2}{\pi}tan^{-1}\left(\frac{zl_x}{A}\right)\right] \quad . \tag{81}$$

Eqns.(72) and (81) represent the resultant electric and magnetic fields, respectively, at a point P on the z-axis due to the electric current present in the conductor.

If the electric current is time-dependent, then both fields are produced; when this happens, each field induces the other in space and as a result of their interactions, electromagnetic disturbances are produced. The appropriate descriptive term for such a disturbance is an electromagnetic wave. The electomagnetic waves propagate with a velocity which is determined by

$$c = \frac{E}{B} \quad , \tag{82}$$

where in air, c has a value of 3×10^8 m/sec, which is the speed of light. Assuming that the electrons composing the electric current travel through the conductor at the speed c, then

$$K = \frac{I}{l_x} = \gamma c \quad , \tag{83}$$

and so the electric field in eqn.(73) and the magnetic field in eqn.(81) satisfy eqn.(82).

Since $E = E_z$ and $B = B_x$, an electromagnetic wave propagates in the y-direction, which is also the direction in which the electric current flows. These electromagnetic waves are radiated everywhere in the air. The radiation pressure due to this electromagnetic radiation is related to the magnitudes of the electric and the magnetic fields by [26]

$$P_r = \frac{1}{2} \left(\frac{B^2}{2\mu_0} + \frac{\varepsilon_0 E^2}{2} \right) \quad , \tag{84}$$

where E and B are the amplitudes of the electric and magnetic fields, respectively. The factor of $1/2$ in eqn.(84) is due to time-averaging. Substituting for E and B from eqns.(71) and (81), respectively, into eqn.(84) gives

$$P_r = \mu_0 \frac{I^2}{l_x^2} \left[1 - \frac{2}{\pi} tan^{-1} \left(\frac{2z}{l_x} \right) - \frac{2}{\pi} tan^{-1} \left(\frac{z l_x}{A} \right) \right]^2 \quad . \tag{85}$$

In time-dependent form, eqn.(85) can be written as

$$P_r(t) = \mu_0 \frac{I^2(t)}{l_x^2} \left[1 - \frac{2}{\pi} tan^{-1} \left(\frac{2z}{l_x} \right) - \frac{2}{\pi} tan^{-1} \left(\frac{z l_x}{A} \right) \right]^2 \quad . \tag{86}$$

So by allowing transient electric currents to pass through the conductor, transient pressure (stress) can also be produced. The piezoelement of the transducer which is assumed to be located at the field point P can also be excited by the electromagnetic radiation.

Assigning the values of $100 mA$, $50 ns$ and $6.35 \times 10^{-4} m$ to $I(t)$, t and z, respectively, the quasi-electrostatic stress and electromagnetic pressure were computed to be $54.2 N/m^2$ and $7.6 \times 10^{-6} N/m^2$, respectively. Therefore, it is expected that the quasi-electrostatic stress would dominate the excitation of the transducer. It should be noted that the values of $I(t)$, t, and z are typical values which will be used later in experimental studies.

EXPERIMENTAL EQUIPMENT

The equipment used for the generation of the input stress pulse signals and the subsequent recording and processing of the transducer's signals is shown schematically in Fig. 13ʹ. The equipment consists of a conducting plate (conductor) cut from brass which is shown in Fig. 14 and the transducer (IQI Model 501) mounted on the conductor through a non-conducting holder which is fabricated from plexiglass. The holder allowed the spacing between the piezoelement and the conductor to be varied from zero to about 1 in (25.4 mm), and it is shown in Fig. 15. Through its electronic unit, the transducer is connected to a variable frequency (1 kHz to 1 MHz) preamplifier (Parametrics Ultrasonic Preamp) of 40 dB gain with 80% accuracy (the 80% accuracy of the preamplifier was determined in the laboratory) and connected to a variable frequency filter (AP-220-5). The output terminal of the filter is connected to a digital oscilloscope (Nicolet 4094A).

Pulse input signals to the transducer are generated by a variable (0 to 24 volts, 0 to 2 amps) direct current (d.c.) supply (Hewlett Packard 628AA) through an astable multivibrator. The electric circuit of the multivibrator is shown in Fig. 16. The circuit consists of a timer (LM 555), two variable resistors, R_A and R_B connected in series, an internal capacitor C_1 and an external capacitor C_2. The output of the multivibrator is connected in series to a load resistor R_L, which limited the output current to a maximum value of 200 mA. 200 mA is the maximum electric current which the internal circuit of the LM 555 can support. The load resistor is serially connected to the conductor of negligible resistance (84 $\times$ 10^{-6} Ω), represented by R_m in the circuit.

When powered, the circuit triggers itself and runs freely as a multivibrator. The external capacitor charges through $R_A + R_B$ and discharges through R_B. Thus, the duty cycle of the circuit is precisely set by the ratio of the two resistors. During this mode of operation, the external capacitor charges and discharges between $1/3\,V_s$

and $2/3 V_s$ where V_s is the voltage of the electrical power source.

The charge time t_1 is given by [27]

$$t_1 = 0.693(R_A + R_B)C_2 \qquad (87)$$

and the discharge time t_2 is given by [27]

$$t_2 = 0.693(R_B)C_2 \quad . \qquad (88)$$

Thus, the total period T is given by the sum of t_1 and t_2, that is,

$$T = 0.693(R_A + 2R_B)C_2 \quad . \qquad (89)$$

A schematic of the output waveforms from the multivibrator is shown in Fig. 17 . The output consists of pulse voltage signals. Each pulse has a width that is equal to t_2 and is reproduced after zero time interval of t_1. The amplitude of each pulse-function is equal to $2/3V_s$.

EXPERIMENTAL PROCEDURE

The values of the two resistors of the astable multivibrator were adjusted such that the recharge, the charge and the discharge times were set at $23\,\mu s$, $0.050\,\mu s$ and $0.45\,\mu s$, respectively. Because the pulse input signals to the transducer consisted of transient stress signals of both electromagnetic and quasi-electrosatic origins, the lower part of the backing was shielded by covering it with aluminum foil. The shielding was done in such a way as to expose only the surface area of the piezoelement to the input signals.

At first, the transducer was mounted as shown in Fig. 11 at a spacing $r = 0.025$ in (0.635 mm) from the conductor. The pulse input signals that were generated and the output (response) of the transducer were captured in the oscilloscope, which was set at a sampling frequency of 50 MHz (one sample per 20 ns) and recorded on a data diskette. The output signals of the transducer were amplified 80 times and highpass filtered from 10 kHz prior to sampling in the oscilloscope. The highpass cut-off frequency of 10 kHz was chosen to eliminate any low frequency noise that existed. In order to ground the transducer, a single wire filament was taped onto the lower face of the backing and stuck out from the holder such that when the electronic unit was covered, the wire made contact with the cover and hence grounded the transducer.

At each incremented spacing of 0.025 in, new measurements of the output signals of the transducer were recorded.

RESULTS AND DISCUSSIONS

Time and frequency domain representations of the outuput voltage signals of the transducer in response to pulse input stress signals of quasi-electrostatic origin are discussed here. Also, the changes in the voltage amplitudes of the output signals in response to changes in the electric current input signals to the conductor as well as to changes in the conductor-piezoelement gap spacing between the conductor and the transducer are discussed. It should be noted that all voltage amplitudes of the output signals are post-amplified signals.

One part of the discussion focuses on the time-domain output signals measured at a spacing of 0.025 in (0.635 mm) between the conductor and the transducer. The time-domain input and output signals are shown in Fig. 18a. The upper trace represents the input signal, while the lower trace represents the impulse response signal of the transducer. In both traces, the voltage amplitudes are represented on the vertical axis, and time is represented on the horizontal axis. From Fig. 18a it can be noticed that for each pulse input signal, there is a corresponding response of the transducer.

For clarity, the expanded form of one step input signal and the transducer's response signal are shown in Fig. 18b. From Fig. 18b, it can be observed that the duration of the pulse input signal is approximaterly 500 ns. This short duration of the input signals is desirable because it is less than the time $t_p = 572$ ns, which is the time required for the input signal to reach the opposite face of the piezoelement. Also, notice that the highest peak-to-peak voltage amplitude of the response signal occurs after time t_p which is the time required for the stress signal to reach the piezoelement-backing interface.

The negligible time-shift of 2.5 ns between the input and output signals is an indication that the quasi-electrostatic forces act on the piezoelement within this time frame. The transducer responds almost instantly to the resulting quasi-electrostatic

33

stress that is generated by the transient electric current passing through the conductor. During this time, transient electromagnetic waves are also produced and the resulting electromagnetic pressure are radiated to the piezoelement. However, it has been pointed out earlier in this report that the magnitude of the electromagnetic pressure is much smaller than the quasi-electrostatic stresse. Therefore, the excitation of the transducer is dominated by the quasi-electrostatic stresses. It is important to mention that if acoustic and mechanical waves were generated during the electrical interaction between the piezoelement and the conductor, the times required for the acoustic wave to transverse the conductor-piezoelement gap spacing of 0.635 mm is 1800 ns while a mechanical wave produced at one end of the conductor requires approximately 1022 ns to arrive at tip of the piezoelement. These times were computed using an acoustic wave velocity of 344 m/s and a surface wave velocity of 2175 m/s in brass. The fact that there are no response signals of the transducer at these time-shifts is an indication that such waves are not responsible for the excitation of the transducer.

Notice that the shape of the input signals is not a perfect rectangle, and hence the response of the transducer is further complicated. The shape of the pulse input signals may have been affected by the time constants of the load resistor R_L connected in series with the output of the excitation circuit R_m (refer to Fig. 16).

The other part of this discussion is devoted to the frequency domain of the output voltage signals. Two typical spectra of one input signal and one output signal are shown in Fig. 18c. The spectra were obtained by a Fast Fourier Transform (FFT) software program. The vertical axis of each spectrum represents the root-mean-square (rms) of the voltage amplitudes, while the horizontal axis represents the frequency in kHz. It can be observed from the plot that the dominant voltage amplitudes of the output spectrum were obtained in a range of frequency between 200 kHz and 2000 kHz. Duke et al. [29] made similar observations when the

34

same type of transducer was used for the ultrasonic characterization of composite materials, in which they reported that the received amplitudes were dominant in a frequency that ranged from 200 kHz to 2000 kHz.

Other characteristics of the transducer can be deduced from the output spectrum. These include the following:

(a) the characteristic or central frequency, which is often denoted by f_0 and defined in [21] as the frequency at which the piezoelement oscillates freely with or without damping.

(b) the quality factor Q, which may be defined as a measure of the sharpness of the resonance of the transducer within its flat sensitivity frequency response range.

The central frequency can be deduced from the output spectrum (see Fig. 18c (b)) to be approximately 600 kHz. The quality factor Q can be expressed as [14]

$$Q = \frac{f_2 - f_1}{f_0} \quad , \tag{90}$$

where f_0 is the central frequency, and f_1 and f_2 are the frequencies corresponding to the two points of intersection of the line

$$V = 0.707 V_c \tag{91}$$

to the spectral curve, where V_c is the voltage amplitude at the central frequency.

Based on the central frequency of 600 kHz, Q was found to be approximately, 0.625. This result is in good agreement with the claim by the manufacturer that Q is less than unity.

The next characteristic feature of the transducer that can be obtained from the output spectrum is the flat amplitude response range, or the sensitivity range. In order to obtain this information, the voltage amplitude has to be converted from its present units [volts] to decibels [dB]. In this report, the conversion was done

by an *FFT-LOG* software program. The *FFT-LOG* program simply converts the voltage amplitudes of the *FFT* plot to decibels by using the formula

$$1 \, dB = 20 \, log \left(\frac{V}{V_0} \right) \quad , \tag{82}$$

where V represents the voltage amplitude in the *FFT*-plot, V_0 is a reference amplitude, which is assigned the value of 1 volt in the *FFT-LOG* program, and *log* represents the logarithm to the base 10.

The *FFT-LOG* plot of the output spectrum is shown in Fig. 18d. The flat amplitude response range is determined by the points of intersection of the line defined by [14]

$$G = G_c \pm 3 \, dB \quad , \tag{93}$$

where G_c is the gain at the central frequency on the *FFT-LOG* curve. The line defined in eqn.(83) intersects the *FFT-LOG* curve at two points corresponding to frequencies of 200 kHz and 1280 kHz. Thus, the sensitivity range of the transducer lies between 200 kHz and 1280 kHz. The manufacturer's claim is that this range is between 50 kHz and 1000 kHz.

One can also define the sensitivity of the transducer relative to the pulse input voltage as [28]

$$R_s = 20 \, log \left(\frac{voltage \, amplitude \, of \, FFT \, plot}{pulse \, input \, voltage \, to \, conductor} \right) \tag{94}$$

where R_s denotes relative sensititvity. Eqn.(94) was used to generate the curve in Fig. 19, which relates R_s to frequency in the region where the dominant voltage amplitudes were received.

The results of the characteristic features of the transducer that are presented here were found to be in good agreement with those obtained from the tone burst characterization technique presented in Appendix A. Note that the tone burst technique is one of the standard characterization methods of ultrasonic transducers.

As an illustration of the similarities in the results obtained from the two methods, consider the output spectra for frequencies between 0 kHz and 3000 kHz obtained from the non-contact and the tone burst techniques, as shown in Figs. 20 and 21, respectively. It is important to note that the similarities of the two spectra lie in their characteristic features over the frequency range and not in the values of the voltage amplitude ratio, which are clearly much higher in the tone burst case than in the non-contact case. This is because the stress input signal of the former is about 400 KN/m^2 while in latter is only 54.2 N/m^2. It is also worth mentioning that the frequency range between 0 kHz and 3000 kHz, which is selected for the comparison, includes the frequency range (200–2000 kHz) where the dominant voltage amplitudes occur.

Based on the output spectrum (see Fig. 21) from the tone burst method, the following results were obtained as the characteristic features of the transducer:

(a) f_0 was found to be approximately 580 kHz, which is about 4% less than that measured by the non-contact method.

(b) Q was found to be approximately 0.85, which is about 36% higher than the value obtained by the non-contact method.

(c) The flat amplitude response ranged from about 200 kHz to 1200 kHz, which compares well with the range of 200 kHz to 1280 kHz that was recorded in the non-contact method case. Therefore, it is justifiable to conclude that the results obtained from the two methods compare favorably.

Having discussed the characteristic features of the transducer, it seems appropriate to extend the discussion to variations of the output voltage amplitude of the transducer with respect to

(a) increases in the pulse input signal (the electric current I), and

(b) changes in conductor-piezoelement gap spacing. To do so requires knowledge of the relationship between the stress $\sigma(t)$ exerted by the quasi-electrostatic

37

forces on the transducer and the two parameters I and z. The expression for $\sigma(t)$ [N/m^2], given in eqn.(75), is

$$\sigma(t) = -\frac{2k\pi I^2(t)\, t^2}{A_c\, A_p} \left[1 - \frac{2}{\pi} tan^{-1} \left(\frac{2z}{l_x} \right) - \frac{2}{\pi} \left(\frac{z l_x}{A} \right) \right] \quad , \tag{95}$$

where k is the coulomb constant, which is given by

$$k = 9 \times 10^9 N - m^2/C^2 \quad . \tag{96}$$

I is the electric current [amperes], z is the spacing [m], and A is given by

$$A = \left[z^2 + (l_y/2)^2 + \frac{l_y}{2} \sqrt{z^2 + (l_x/2)^2 + (l_y/2)^2} \right] \quad . \tag{97}$$

The output voltage amplitude was also shown to be related to σ_i (see eqn.(49)) according to

$$V(t) = \frac{2\sigma(t)\, h\, t_d}{Z_a + Z_p} \left[\frac{(\tau_2)\, exp(-t\tau_2) - (\tau_1)\, exp(-t\tau_1)}{\tau_2 - \tau_1} \right] \quad , \tag{98}$$

where

$$\tau_1, \tau_2 = -\frac{1}{2RC_0} \pm \left[\left(\frac{1}{2RC_0} \right) + \frac{h^2}{RA_p(Z_a + Z_p)} \right]^{\frac{1}{2}} \quad . \tag{99}$$

The quantity τ has unit of 1/s, the time t and the duration t_d of the pulse signal have units of seconds. The quantity h [volts/m] is the piezoelectric deformation constant, A_p [m^2] is the surface area of the piezoelement tip, and R [ohms] and C_0 [farads] are the resistance and the capacitance of the piezoelement, respectively. The characteristic impedances of the propagation medium and of the piezoelement are given by Z_a and Z_p, respectively. The propagation medium is air and its characteristic impedance Z_a is approximately equal to zero [21]. All other constant parameters of the transducer entering eqn.(98) are listed in Table 1.

Eqn.(98) can be written as

$$V(t) = C\sigma(t) \quad , \tag{100}$$

where C is the global constant which can be defined as

$$C = -\frac{2h\,t_d}{Z_p}\left[\frac{(\tau_2)\,exp(-t\tau_2) - (\tau_1)\,exp(-t\tau_1)}{\tau_2 - \tau_1}\right] \quad . \qquad (101)$$

Combining eqns.(96) and (100) gives

$$V(t) = C'I^2\left[1 - \frac{2}{\pi}tan^{-1}\left(\frac{2z}{l_x}\right) - \frac{2}{\pi}tan^{-1}\left(\frac{zl_x}{A}\right)\right] \quad , \qquad (102)$$

where C' is a constant of proportionality that is given by

$$C' = C\frac{2k\pi}{A_c\,A_p} \quad . \qquad (103)$$

Eqn.(102) shows that the output voltage amplitude of the transducer is proportionally related to the square of the input electric current in the conductor and the output voltage amplitude is related to the spacing of the conductor-piezoelement gap through an inverse tangent function.

By choosing the value of t equal to t_p and by keeping z constant, plots of theoretical and experimental curves of V versus I were generated, as shown in Figs. 22 and 23, respectively. In Fig. 23, V is the measured peak-to-peak amplitude of the output voltage signal of the transducer.

Similarly, by keeping I constant and t equal to t_p, plots of theoretical and experimental curves of V versus z were generated in the time domain as shown in Figs. 24 and 25, respectively. In the frequency domain, the experimental plot of V versus z is shown in Fig. 24. In the frequency domain, the output voltage amplitudes were measured at the central frequency of the output spectra obtained at the different spacings of the transducer from the conductor.

Notice that from Fig. 23, even though the square law which relates V to I is not quite generated, there are similarities between this experimental curve and the predicted curve in Fig. 22. The experimental curve is approximately linear. From Figs. 24 and 25, it can be observed that the similarities between the theoretical and

experimental curves are much closer. The drop in the voltage amplitude between zero and one inch spacings is about 30% higher in the experimental curve than it is in the theoretical curve. This implies that the piezoelement of the transducer may not have been completely isolated from external interferences.

It is interesting to notice that the observed voltage amplitudes were the same order of magnitude as those predicted by eqn.(98). For example, at a spacing of $r=0.025$ in, the predicted value for $V(t)$ is about 6.350 mV while that measured experimentally is about 5.625 mV. Therefore, the observed voltage amplitudes are within 10% of the theoretically predicted voltage amplitudes.

CONCLUSIONS AND RECOMMENDATIONS

A dynamic surface displacement transducer (IQI Model 501) has been characterized by a new non-contact characterization technique. The technique involved exciting the transducer by pulse stress signals of quasi-electrostatic origin.

A theoretical model was presented which sought to predict the behavior of piezoelectric transducers when they are subjected to transient pulse stress signals. Also, the physical principle for generating the stress signals of quasi-electrostatic origin was presented.

Experimentally, the quasi-electrostatic forces were generated by transient electric currents that were allowed to pass through a brass plate which was located at specified distances from the transducer. The impulse response (output) signals of the transducer were monitored using a digital oscilloscope from which they were later studied in both the time and the frequency domains.

In the time domain, the highest peak-to-peak output voltage amplitude was observed to occur approximately after a time $t = t_p$ ($t_p = L_p/c_p$, where L_p and c_p are the thickness of the piezoelement and the wave speed in the piezoelement, respectively). This is true for all the pulse input signals. The absence of any significant signals after this period for any input is an indication that the piezoelement and the backing are in excellent impedance match. This observation supports the reports in the literature that the acoustic impedances of the piezoelement (PZT-5A) and the backing (brass) differ by approximately only 1.7%.

In the frequency domain, the results derived from the spectrum of the output signal of the transducer showed that

(a) the central frequency f_0 of the transducer was approximately 600 kHz;

(b) the quality factor Q was approximately 0.625;

(c) the flat amplitude response range was from 200 kHz to 1280 kHz; and

(d) the dominant output voltage amplitudes were received for frequencies that ranged from 200 kHz to 2000 kHz.

All the results compare favorably to those obtained additionally by the tone burst method which is one of the conventional methods for characterizing ultrasonic and acoustic emission transducers. This method is presented in Appendix A of this report.

With the exception of the flat amplitude response range, which according to the manufacturer is from 50 kHz to 1000 kHz, all other characteristic features of the transducer are in good agreement with those claimed by the manufacturer.

Other advantages of the non-contact method include:

(a) the fact the experimentally measured voltage amplitudes obtained were found to be about 10% less than the theoretically predicted values;

(b) the simple experimental setup which is both controllable and reproducible and with fast repetition rate; and

(c) the low cost of the excitation circuit whose estimated cost together with the power supply is less than 100 U.S. dollars. These advantages of this new characterization technique of ultrasonic and acoustic emission transducers indicate that the technique is reliable and has potential applications in sensor calibrations.

In concluding this report, a recommendation concerning the design of the electronic unit of the transducer is necessary. The present design is very delicate and, therefore, it is very easily disturbed or damaged. For instance, most of the electrical contacts are exposed. It would have been better if the transducer were built as a secure and sturdy black box.

REFERENCES

[1] W. P. Mason, Electromechanical Transducers and Wave Filters (second edition), D. van Nostrand Company, Inc., 1948.

[2] T. L. Ryne, "An Improved Interpretation of Mason's Model for Piezoelectric Plate Transducers", IEEE Transactions on Sonics and Ultrasonics, Vol. SU-25, No. 2, March 1978, pp 98 − 103.

[3] W. M. R. Smith and A. D. Awojobi, "Factors in the Design of Ultrasonic Probes", Ultrasonics, Vol. 17, pp 20 − 26.

[4] G. Kossoff, "The Effects of Backing and Matching on the Performance of Piezoelectric Ceramic Transducers", IEEE Transactions on Sonics and Ultrasonics, Vol. SU-13, No. 1, March 1966, pp 20 − 30.

[5] E. K. Sittig, "Effects of Bonding and Electrode Layers on the Transmission Parameters of Piezoelectric Transducers used in Ultrasonic Digital Delay Lines", IEEE Transactions on Sonics and Ultrasonics, Vol. SU-16, No. 1, January 1969, pp 2 − 10.

[6] R. W. Martin and R. A. Siegelmann, "Force and Electrical Thevinin Equivalent Circuits and Simulations for Thickeness Mode Piezoelectric Transducers", Journal of the Acoustical Society of America, Vol. 58, No.2, August 1975, pp 475 − 489.

[7] R. Krimholtz, D. Leedom, and G. Matthaei, "New Equivalent Circuits for Elementary Piezoelectric Transducers", Electronics Letters, Vol. 6, June 1970, pp 398 − 399.

[8] C. S. Desilets, J. D. Fraser, and G. S. Kino, "The Design of Efficient Broad-Band Piezoelectric Transducers", IEEE Transactions on Sonics and Ultrasoics, Vol. SU-25, No. 23, May 1978, pp 115 − 125.

[9] D. Dotti, "A New Model of a Piezoelectric Transducer for Direct Impulse Response Evaluation", IEEE Transactions on Sonics and Ultrasonics, Vol. SU-22,

No.3, May 1975, pp 202 − 205.

[10] M. Redwood, "Transient Performance of a Piezoelectric Transducer", Journal of the Acoustical Society of America, Vol. 33, No. 44, April 1961, pp 527−536.

[11] M. Redwood, "A Study of Waveforms in the Generation and Detection of Short Ultrasonic Pulses", Applied Materials Research, Vol. 2, April 1963, pp 76−84.

[12] J. H. Williams, Jr. and B. Doll, "A Simple Wave Propagation Analysis of Piezoelectric Ultrasonic Transducer Response", Materials Evaluation, Vol. 40, No. 13, December 1982, pp 1374 − 1381.

[13] S. S. Lee and J. H. Williams, Jr., "Stress Wave Attenuation in Thin Structures by Ultrasonic Through Transmission", Journal of Nondestructive Evaluation, Vol. 1, No. 4, April 1980, pp 277 − 285.

[14] W. Sachse and N. N. Hsu, "Ultrasonic Transducers for Materials Testing and Their Characterization", Physical Acoustics, Vol. 14 (W. P. Mason and R. Thurston editions), Academic Press, New York, 1979, pp 277 − 406.

[15] F. R. Breekenbridge, C. E. Tschiegg, and M. Greenspan, "Acoustic Emission: Some Applications of Lamb's Problem", Journal of the Acoustical Society of America, Vol. 57, No. 3, March 1975, pp 626 − 631.

[16] N. N. Hsu, J. A. Simmons, and S. C. Hardy, "An Approach to Acoustic Emission Signal Analysis", Materials Evaluation, Vol. 35, No. 11, October 1977, pp 100 − 106.

[17] H. Hatano, "Quantitative Measurements of Acoustic Emission Related to Its Microscopic Mechanisms", Journal of the Acoustical Society of America, Vol. 57, No. 3, March 1975, pp 639 − 645.

[18] W. J. Pardee and L. J. Graham, " Frequency Analysis of Two Types of Simulated Acoustic Emissions", Journal of the Acoustical Society of America, Vol. 63, No. 3, March 1978, pp 793 − 799.

[19] S. L. Bride and T. S. Hutchinson, "Absolute Calibration of Helium Gas Jet

Noise Source", Canadian Journal of Physics, Vol. 56, 1978, pp 504 − 507.

[20] D. M. Egle and A. E. Brown, "A Note on Pseudo-Acoustic Emission Sources", Journal of Testing and Evaluation, Vol.4, No. 3, 1976, pp 196 − 199.

[21] J. Krautkramer and H. Krautkramer, Ultrasonic Testing of Materials (third edition), Springer-Verlag, New York, 1983.

[22] S. C. U. Ochi and J. H. Williams, Jr., "One Dimensional Wave Propagation in Rods of Variable Cross Section: A WKBJ Solution ", Composite Materials and Nondestructive Evaluation Laboratory, Massachusetts Insitute of Technology, 1987.

[23] J. H. Williams, Jr. and S. C. U. Ochi, "Wave Propagation in Isotropic Elastic Rods of Variable Cross Section", Composite Materials and Nondestructive Evaluation Laboratory, Massachusetts Institute of Technology, 1987.

[24] J. H. Williams, Jr., H. Nayeb-Hashemi, and S. S. Lee, "Attenuation and Velocity in AS:3501-6 Graphite Fiber Composite", Journal of Nondestructive Evaluation, Vol. 1, No.2, 1980, pp 137-148.

[25] E. Kreyszis, Advanced Engineering Mathematics (fourth edition), John Wiley & Sons, 1979.

[26] F. W. Sears, M. W. Zemansky, and H. D. Young, University Physics, Part II (fifth edition), Addison-Wesley Publishing Co., London, 1976.

[27] Linear Databook, National Semiconductor, 1984.

[28] Wave Form Analysis, Nicolet Instrument Corportation, 1985.

[29] J. C. Duke, Jr., E. G. Henneke II, and W. W. Stinchcomb, "Ultrasonic Stress Wave Characterization of Composite Materials", NASA CR-3976, May 1986.

[30] T. M. Proctor, Jr., "Improved Piezoelectric Acoustic Emission Transducer", Journal of the Acoustical Society of America, Vol. 71, No. 15, May 1982, pp 1163-1168.

Table 1

Some Constant Parameters of Piezoelement (PZT-5A).

Quantity	Name	Units	Value
h	Piezoelectric deformation constant	V/m	2.15×10^9
g	Piezoelectric voltage constant	Vm/N	24.8×10^{-3}
d	Piezoelectric strain constant	C/N	374×10^{-12}
ρ_R	Volume resistivity	Ω m	10^{11}
R*	Resistance	Ω	10^{15}
C_o^*	Capacitance	pF	10.63
s*	Surface contact area	m^2	7.00×10^{-6}
ϵ	Relative dielectric constant	-	1700
ρ_p	Mass density	Kg/m^3	7.75×10^3
Zp	Characteristic impedance	Kg/m^2sec	36.5×10^6
cp	Wave speed	m/s	4350
Tc	Curie temperature	°C	365

* Calculated parameters from the geometry of the piezoelement.
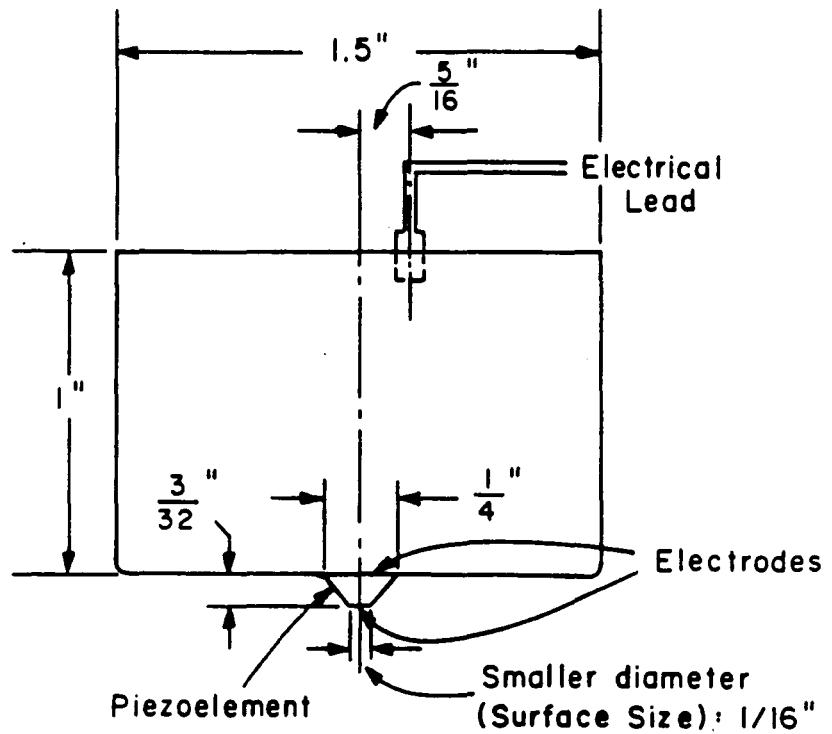
Fig. 1 Schematic of transducer (IQI model 501) without plastic shield.
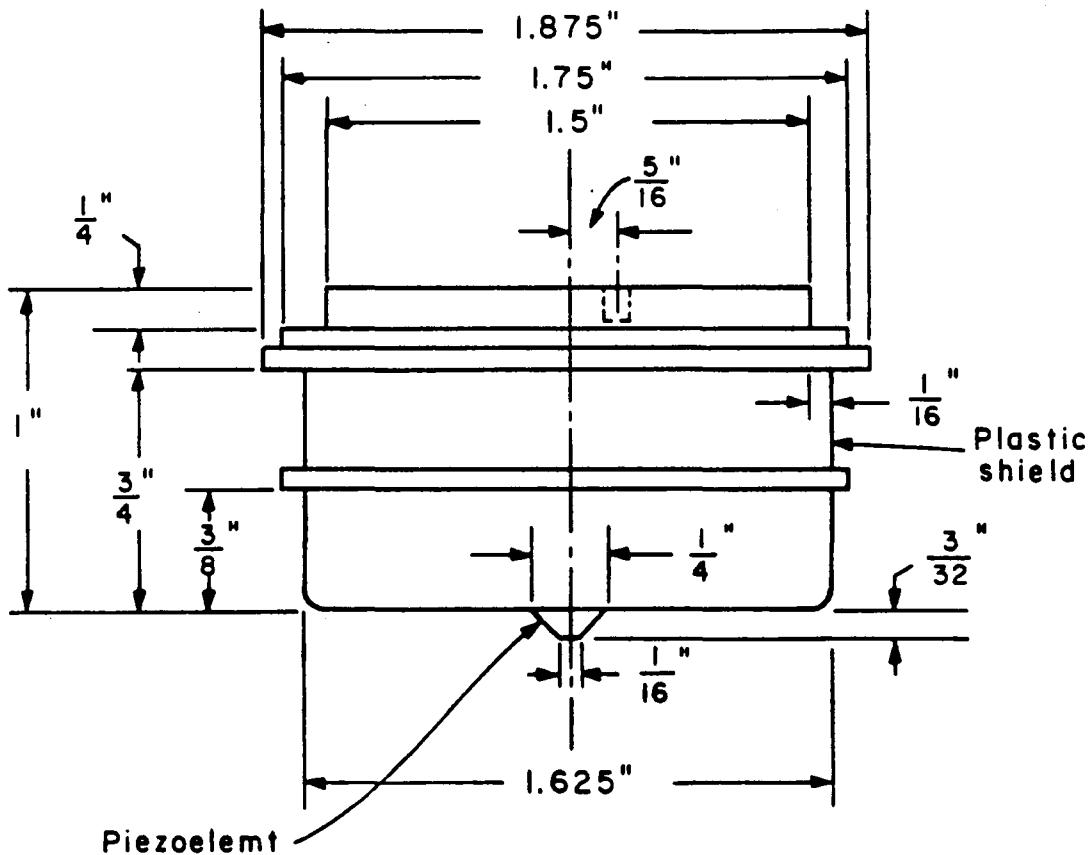
Fig. 2 Schematic of transducer (IQI model 501) with plastic shield.

+ V$_e$

3.3MΩ

6.8MΩ

10μF

OUTPUT

2

7

LF351

3

6

4

Operational
Amplifier

39Ω

3

LF0002
CN

1

8

Current
Amplifier

4.7μF

0.02μF

INPUT

10MΩ

10MΩ

0.1μF

10kΩ

− V$_e$
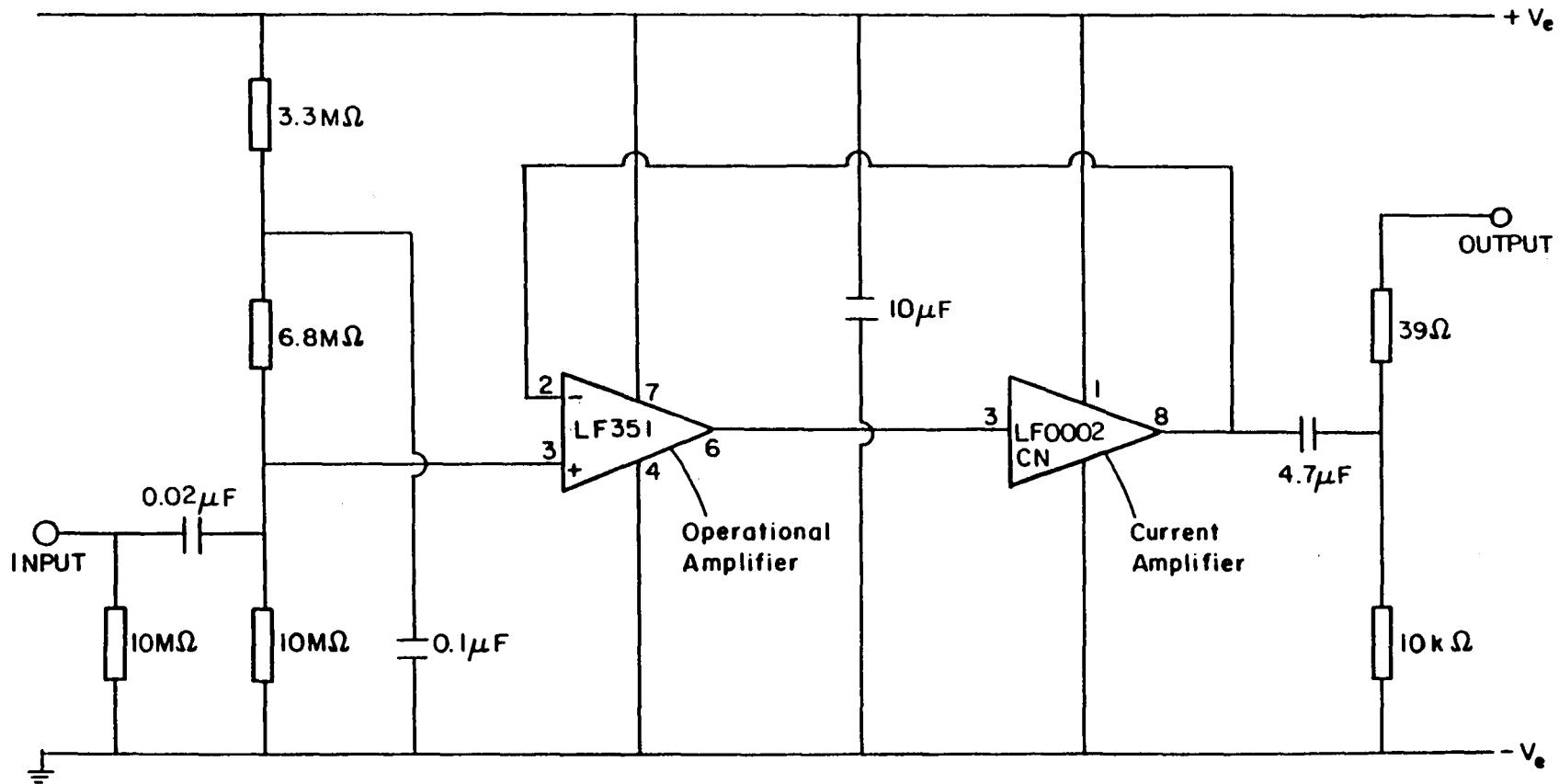
Fig. 3 Electric circuit of transducer amplifier.
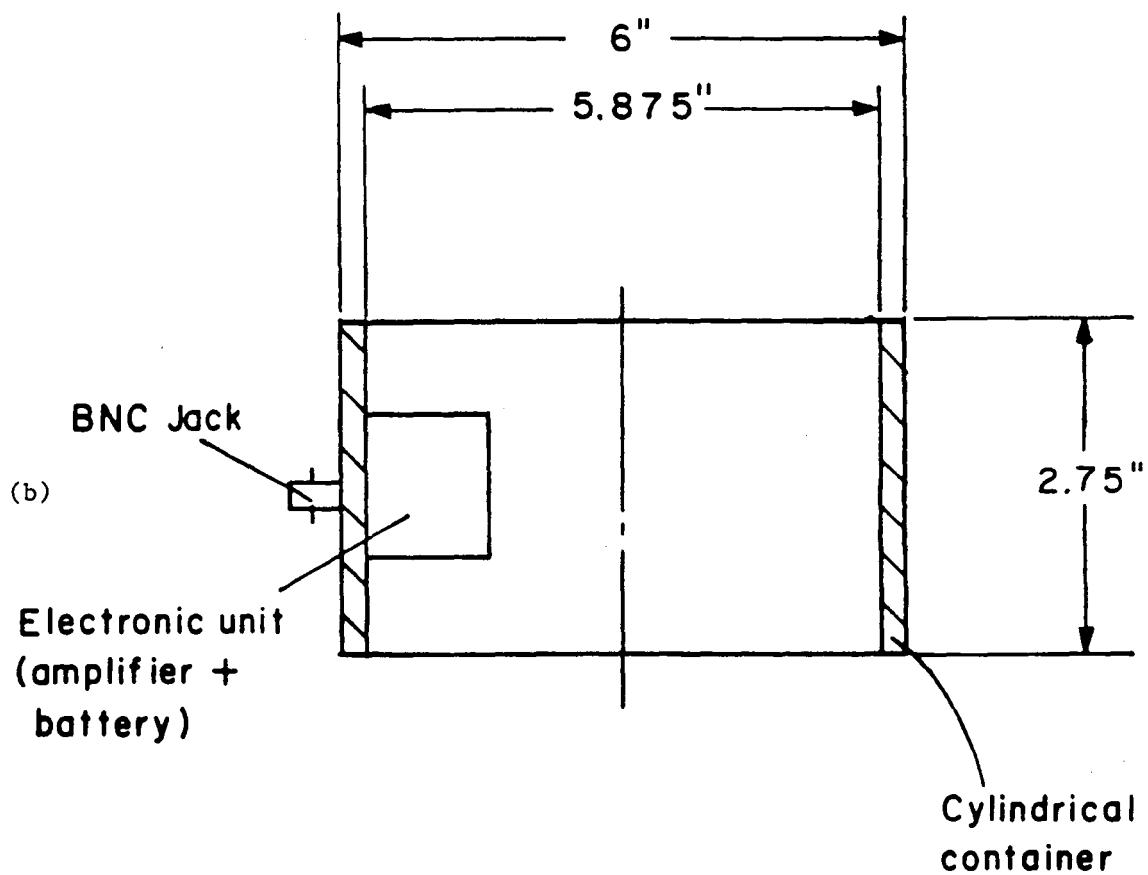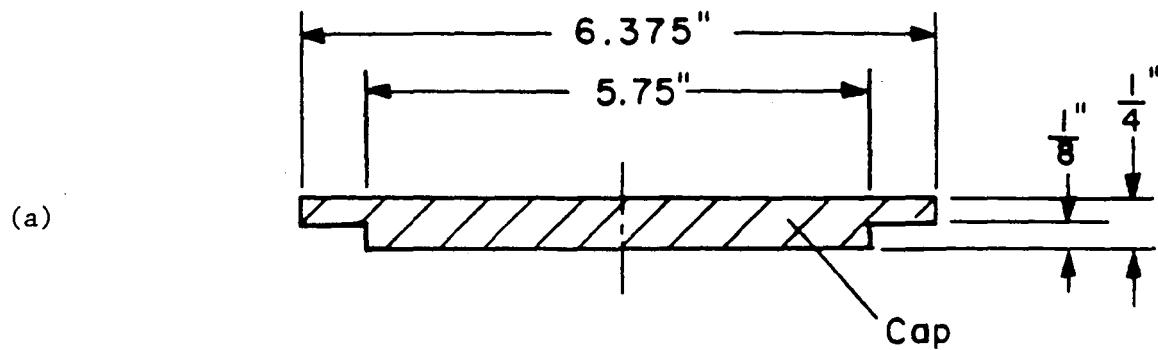
Fig. 4 Schematics of

       (a) cap of electronic unit; and

       (b) cylindrical container on which amplifier and battery are mounted.
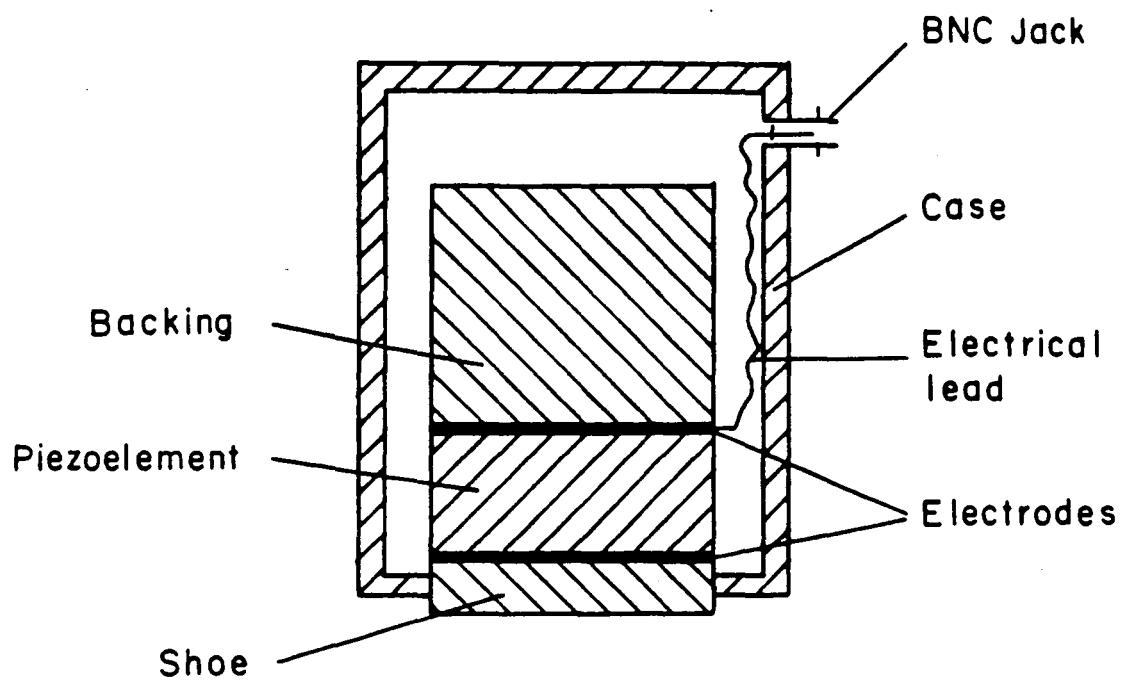
Fig. 5   Schematic of conventional pulse/echo piezoelectric transducer.
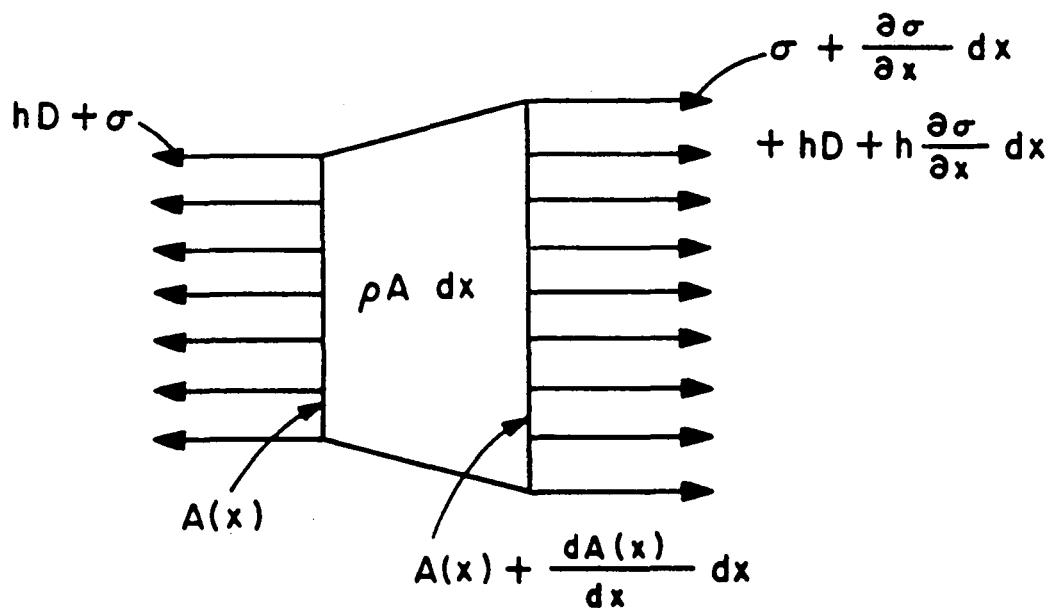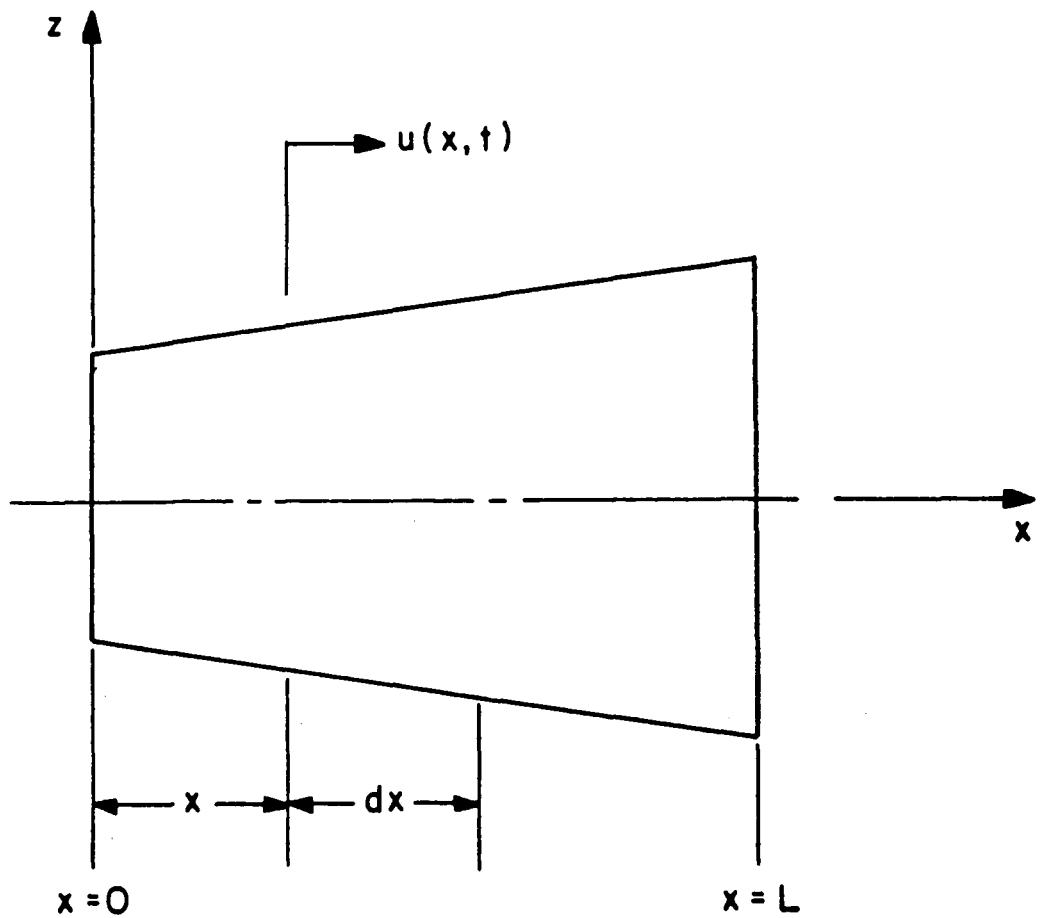
Fig. 6   Piezoelectric rod of variable cross section supporting
          longitudinal wave propagation in x-direction.

52
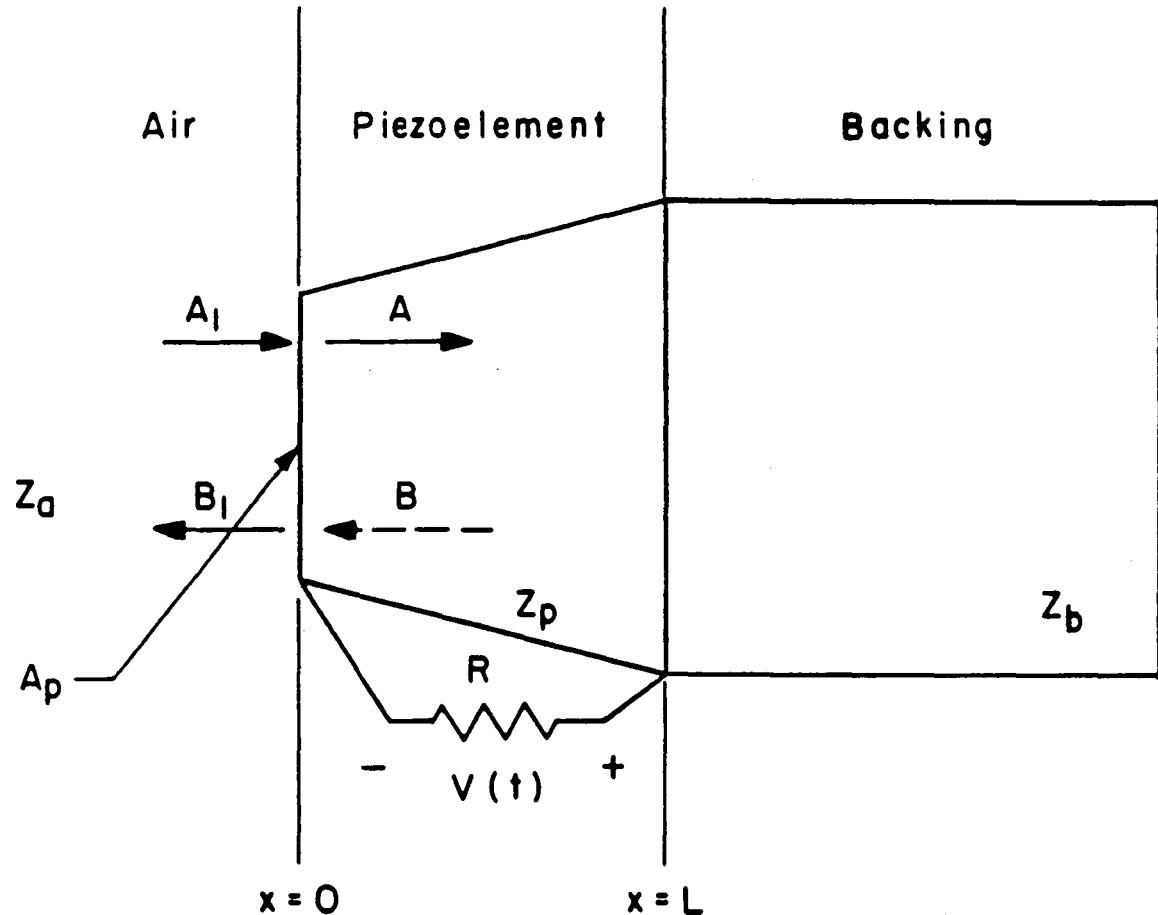
Fig. 7   Two layer piezoelectric transducer used to detect ultrasonic waves.
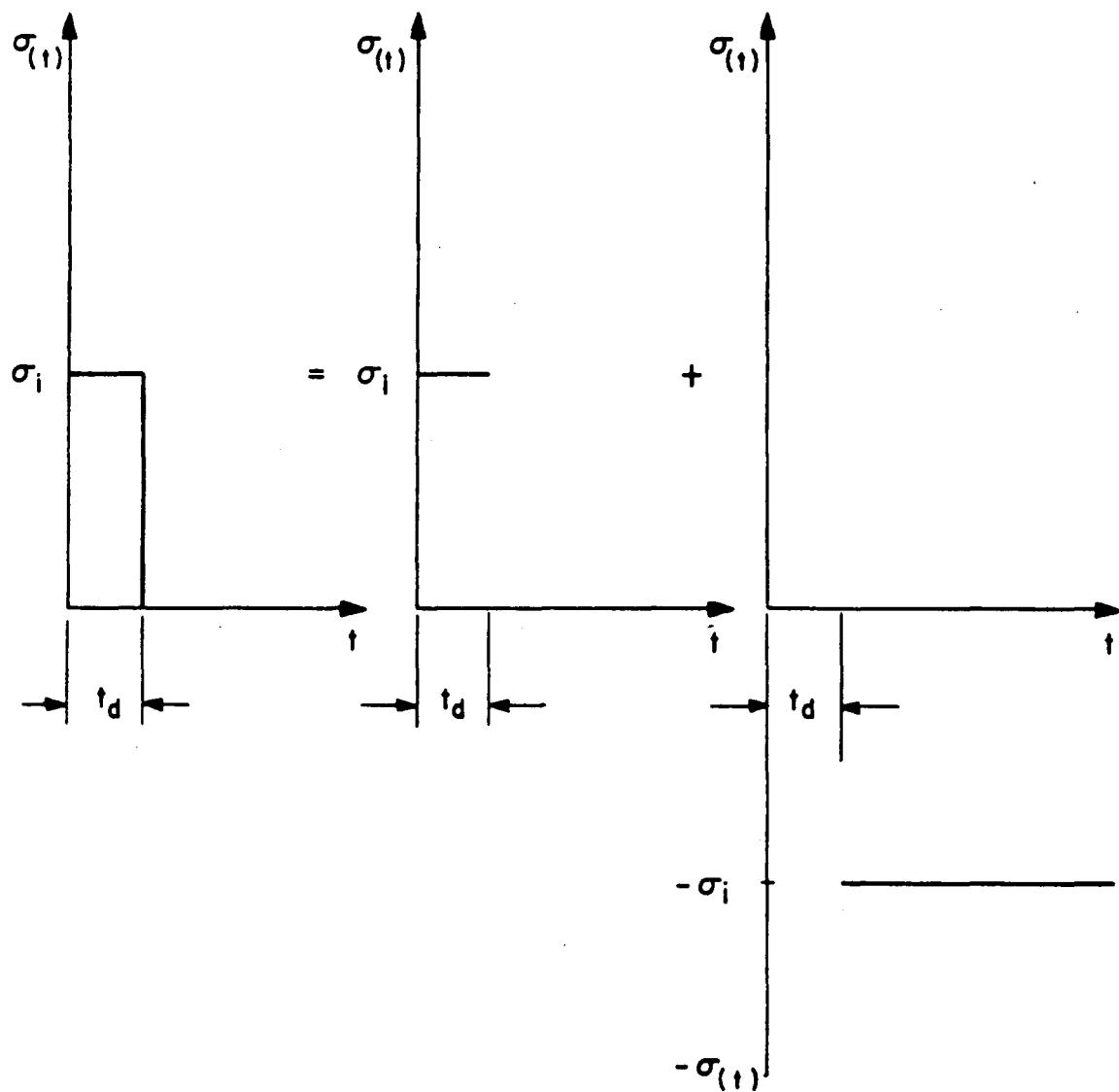
Fig. 8   Schematic of pulse stress function.
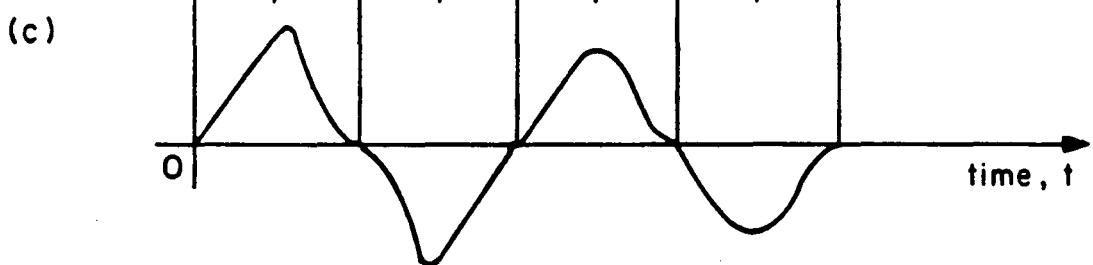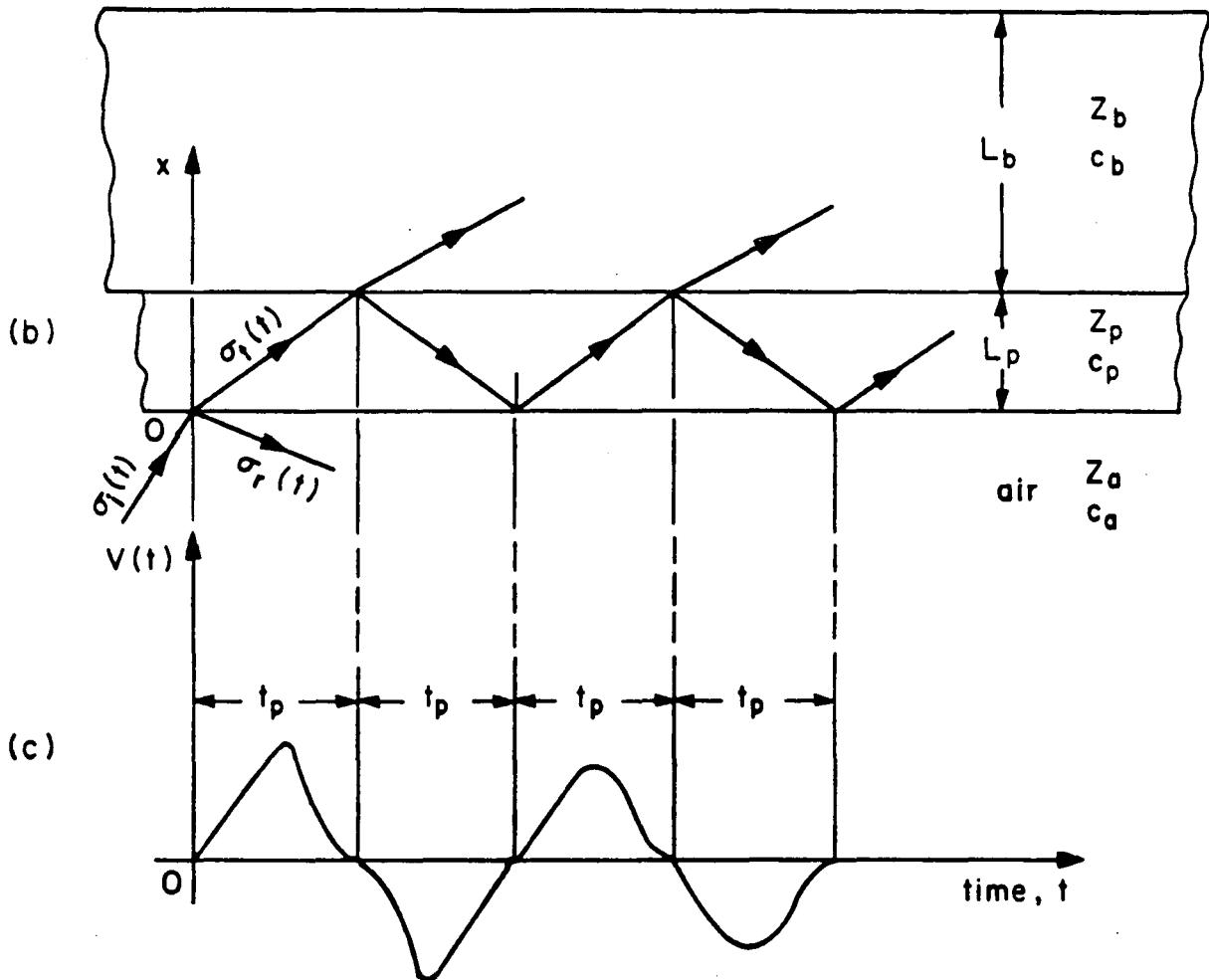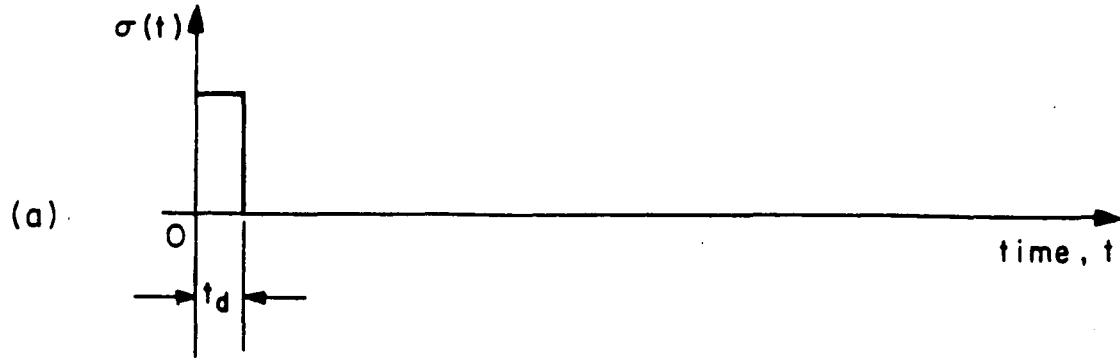
Fig. 9 Schematics of
(a) pulse/stress input signal to transducer;

(b) two-component layer of transducer: piezoelement and backing; and

(c) response of transducer.

55
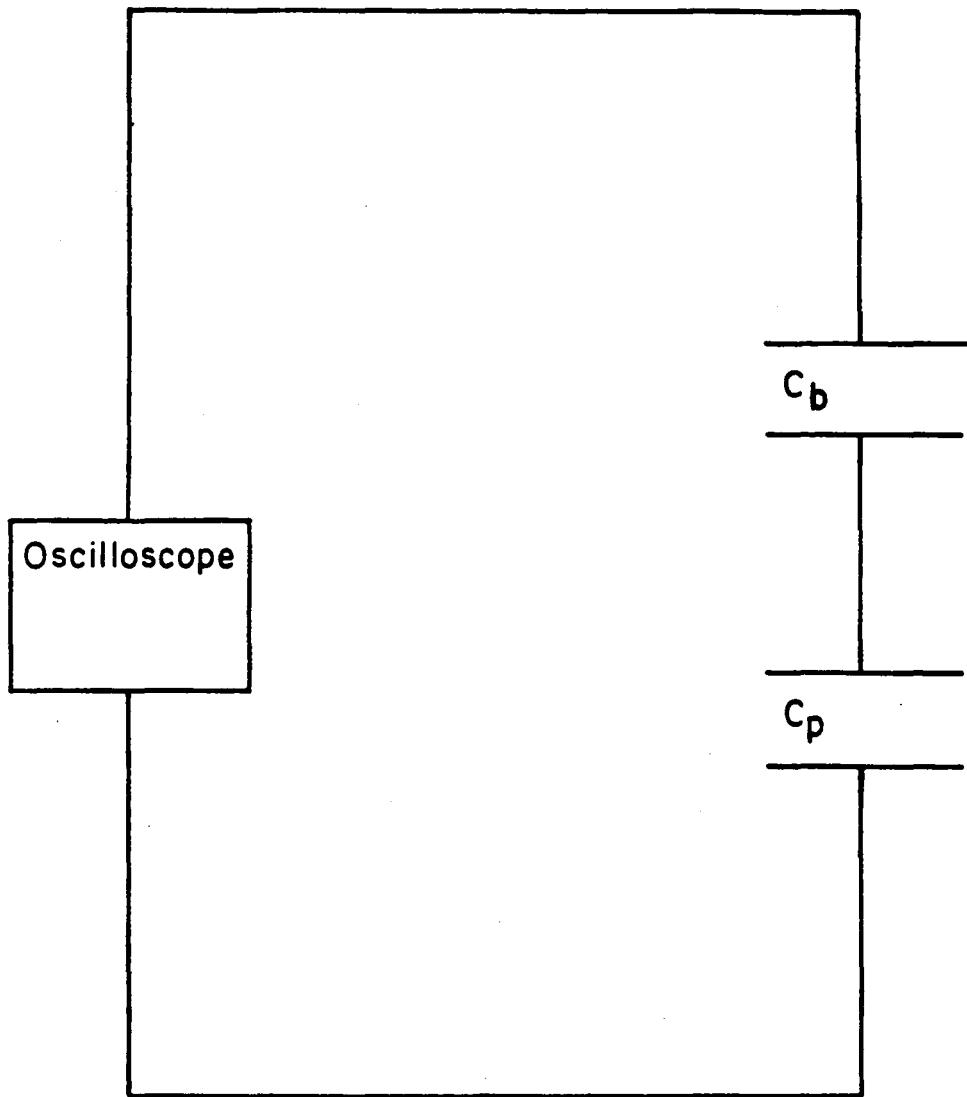
Fig. 10   Electrical circuit model of piezoelement (C_p) and backing (C_b) as two parallel-plate capacitors connected in series to oscilloscope.
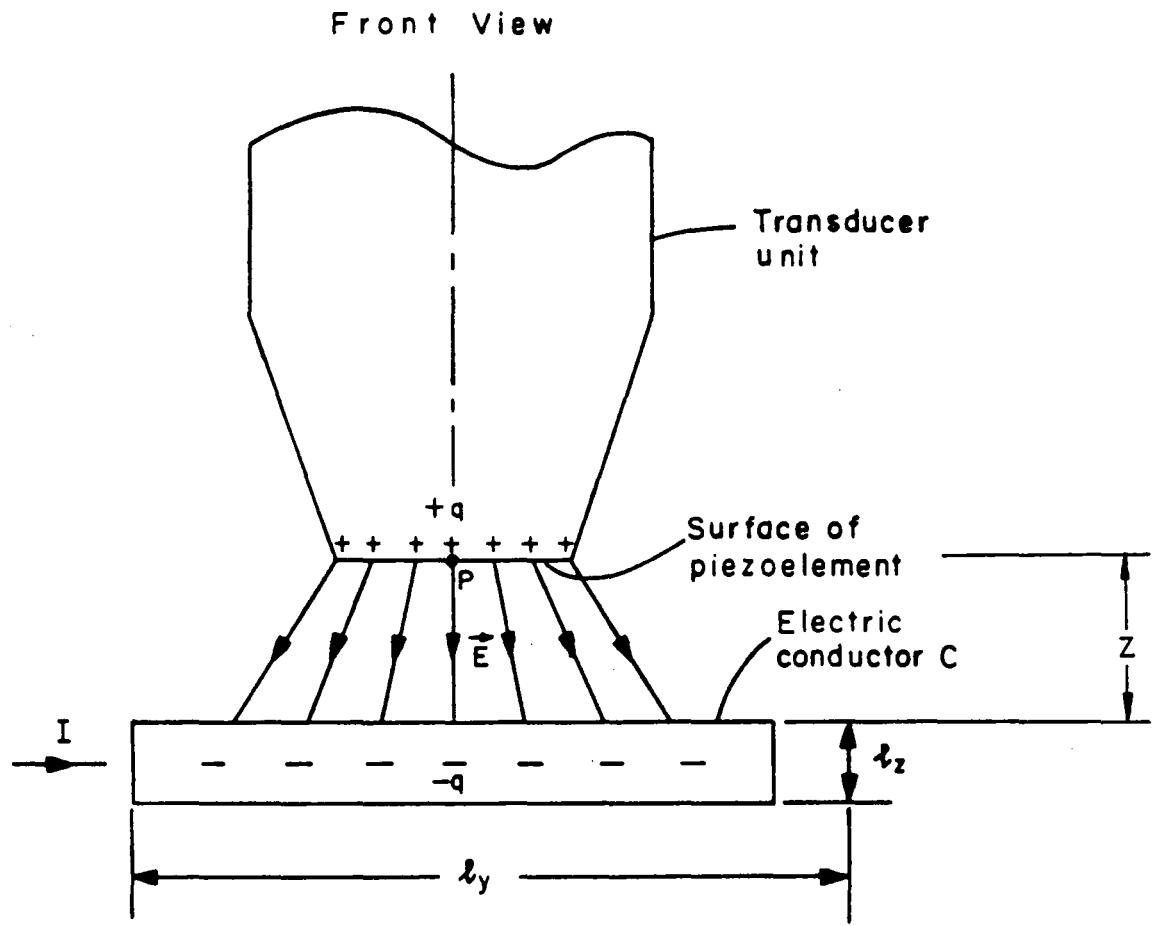
Fig. 11 Schematic of electric field between piezoelement and electric conductor showing distribution of electric charges.
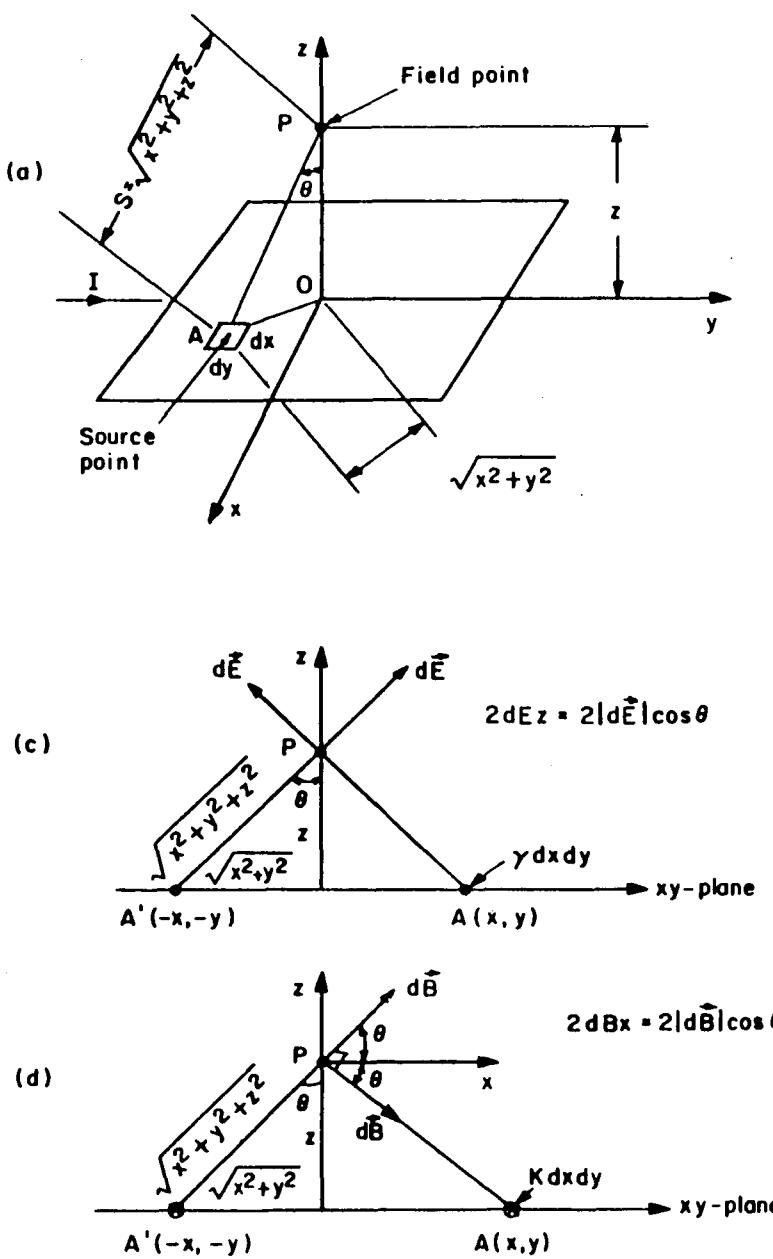
Fig. 12 Schematics of

(a) rectangular electric conductor of dimensions l_x and l_y, supporting electric current of magnitude I;

(b) same conductor showing dimensions in xy plane;

(c) electric field at point P (in x-z plane) due to charge element $\gamma dxdy$; and

(d) magnetic field at point P (in x-z plane) due to current element Kdxdy.
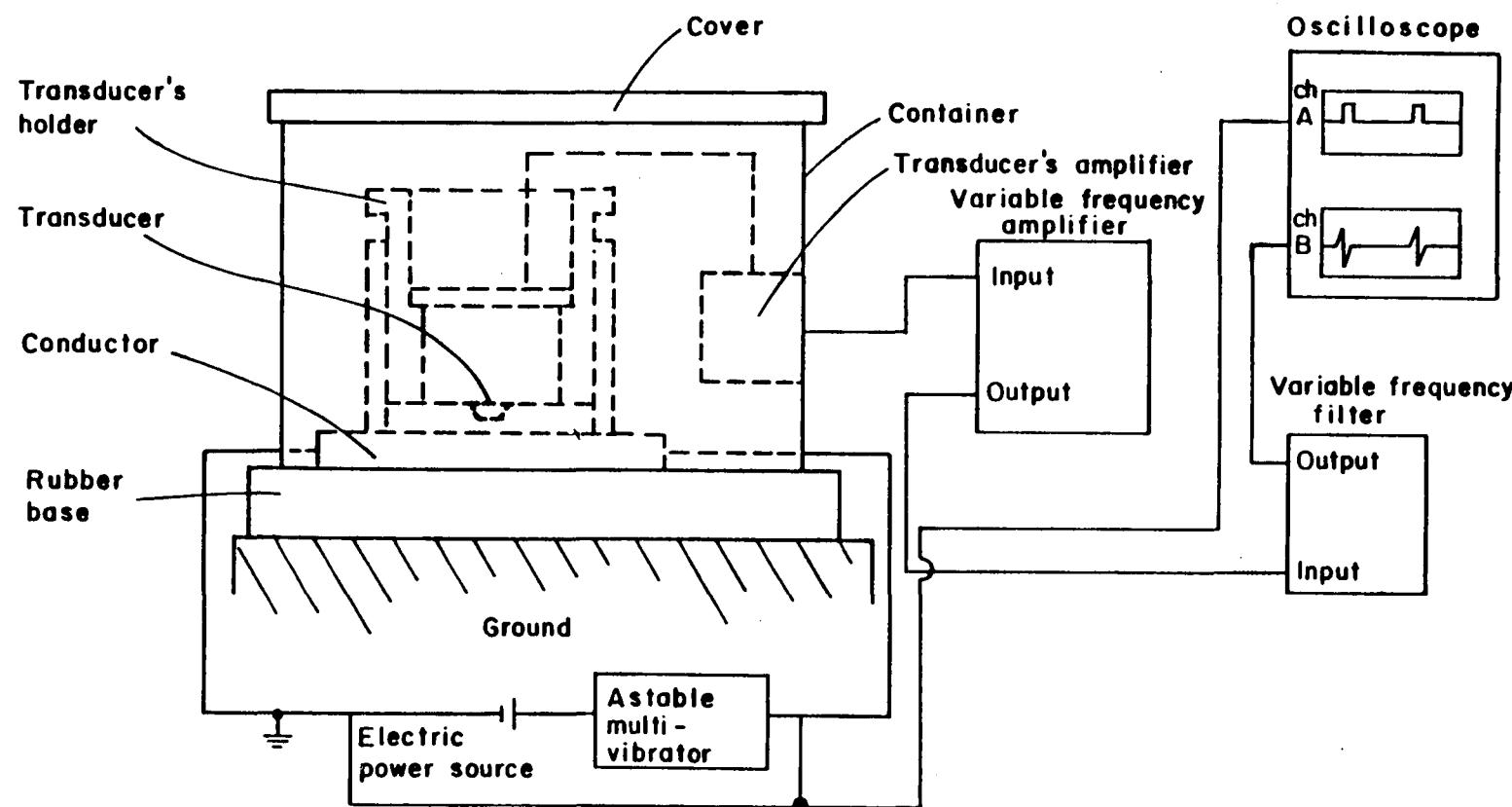
Fig. 13   Schematic of measuring equipment.
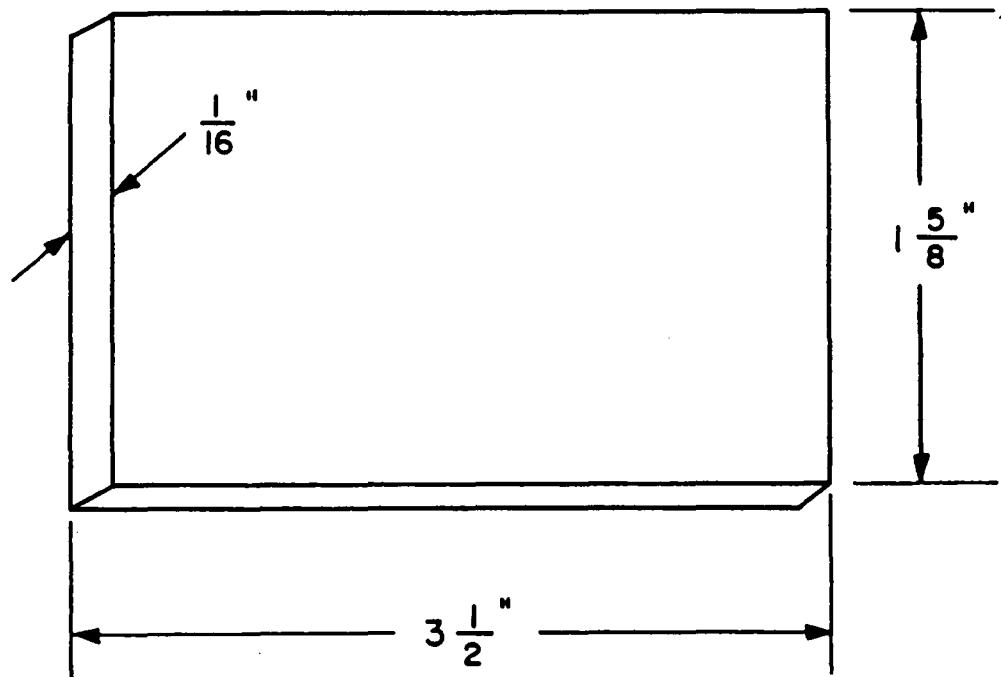
Fig. 14   Schematic of conductor.

(a)

(b)
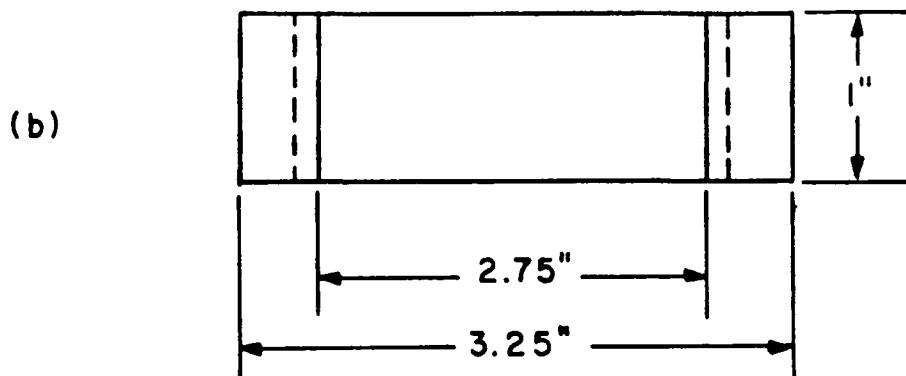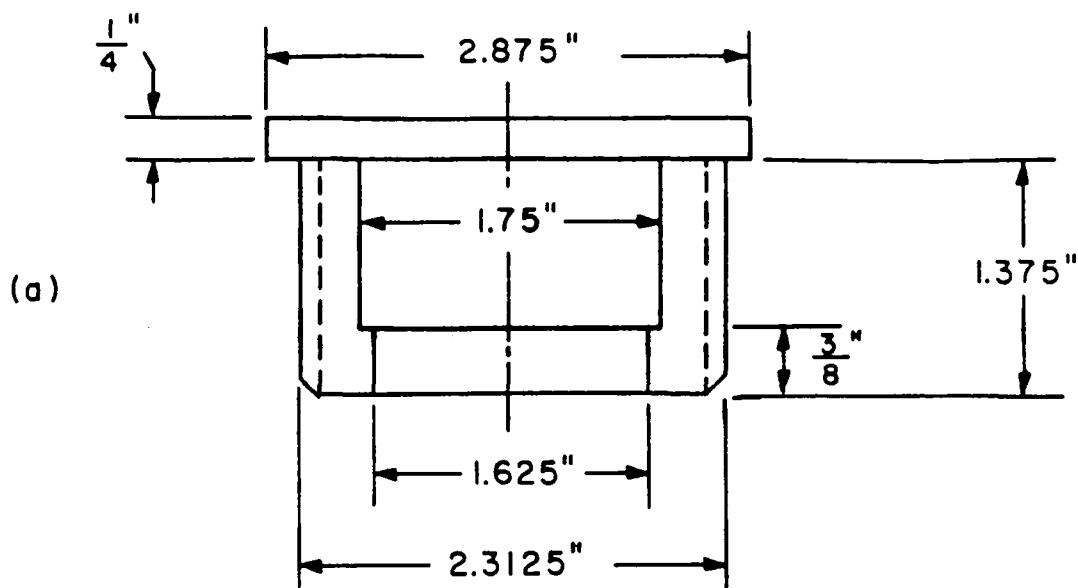
Scale 1:1

Fig. 15   Schematics of transducer's holder:

(a) Screw [material: plexiglass]; and

(b) Nut [material: plexiglass].

61
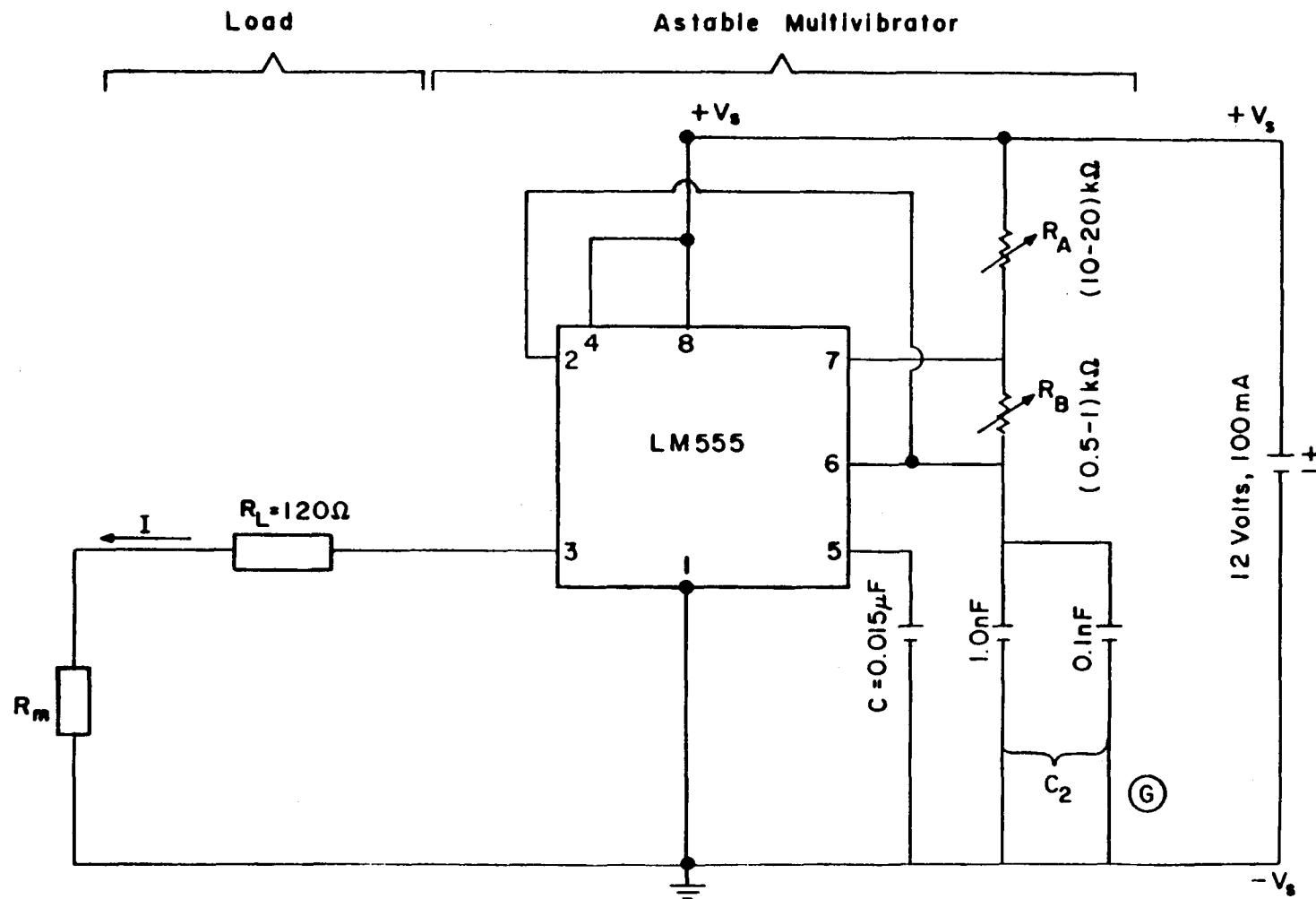
Fig. 16 Electrical circuit for generating pulse-input signals to metallic plate.
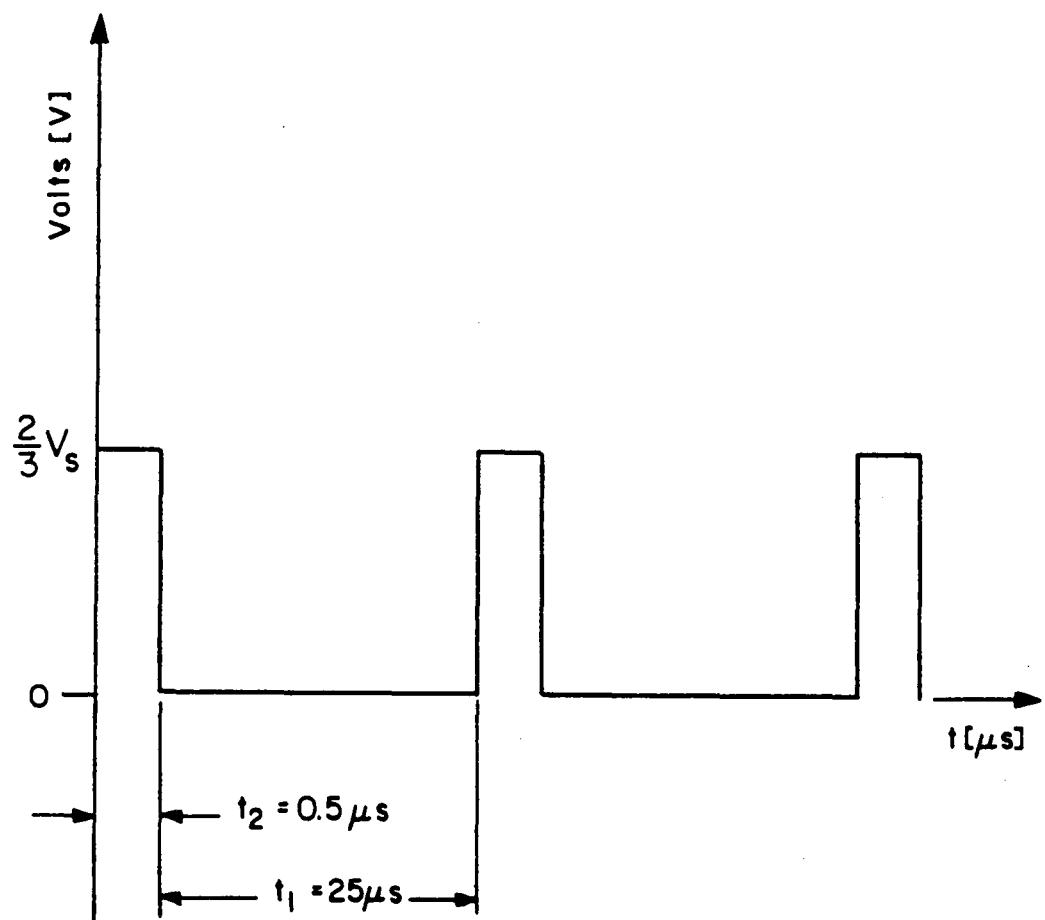
Fig. 17 Schematic of output waveform from the multivibrator.
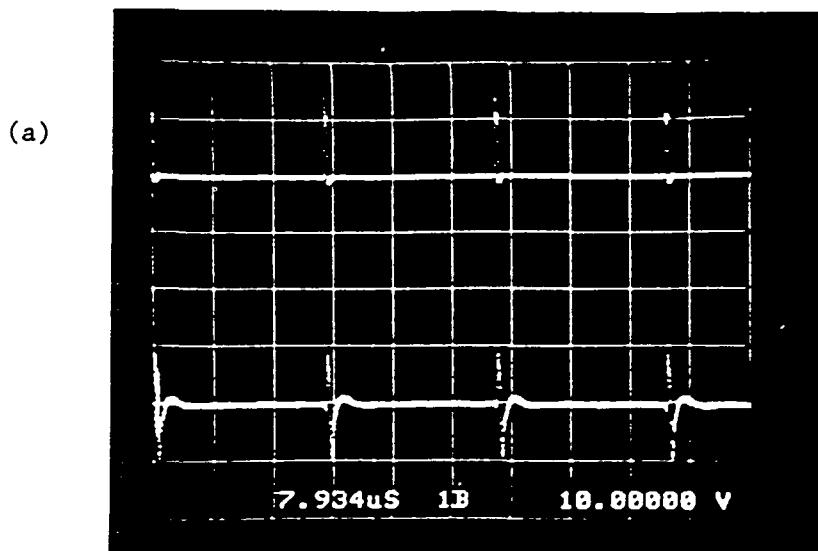
(a)

Input trace

Vertical scale: 10 V/Div.
Horizontal scale: 7.934 us/Div.

Output trace

Vertical scale: 250 mV/Div
Horizontal scale: 7.934 us/Div.

(b)
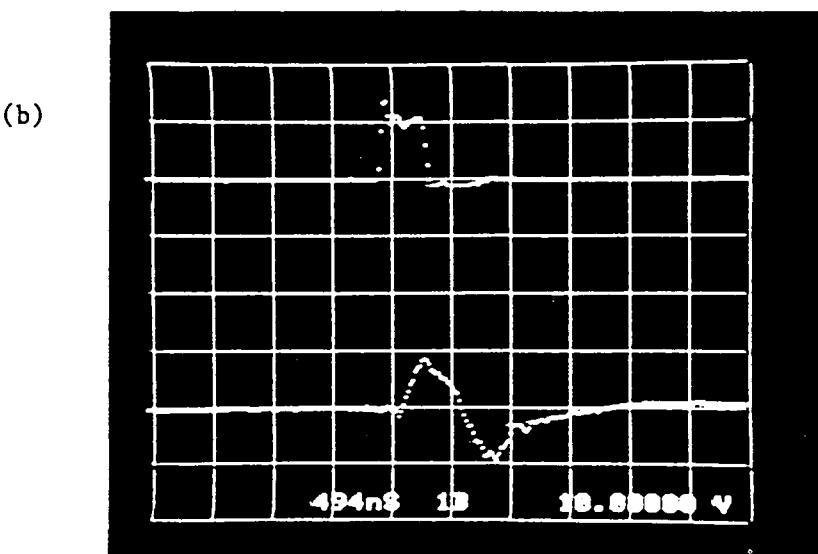
Input trace

Vertical scale: 10 V/Div.
Horizontal scale: 494 ns/Div.

Output trace

Vertical scale: 250 mV/Div.
Horizontal scale: 494 ns/Div.

Fig. 18   (a) Pulse input signals and impulse responses of transducer; and

(b) Expanded form of one pulse input signal and corresponding impulse
response of transducer.

(i)
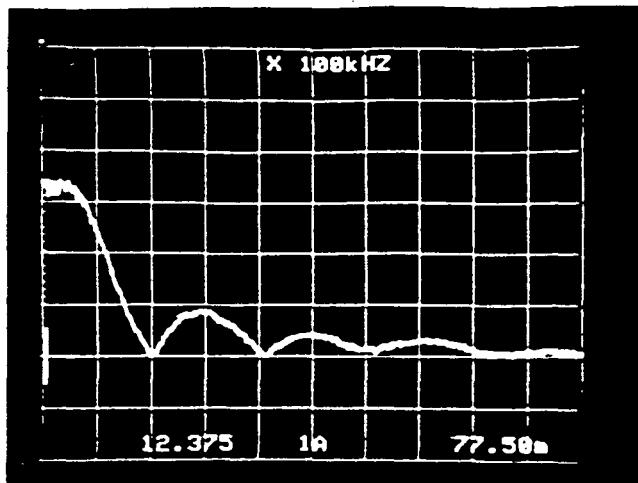
Input spectrum

Vertical scale: 77.50 mV/Div.
Horizontal scale: 1237.5 kHz/Div.

(ii)
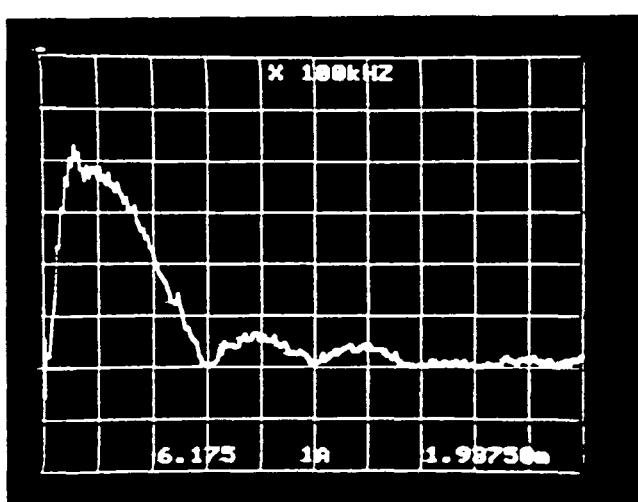
Output spectrum

Vertical scale: 1.9375 mV/Div.
Horizontal scale: 617.5 kHz/Div.

Fig. 18(c)   FFT plot of

(i) one pulse input signal to transducer; and
(ii) one impulse response signal of transducer.

65
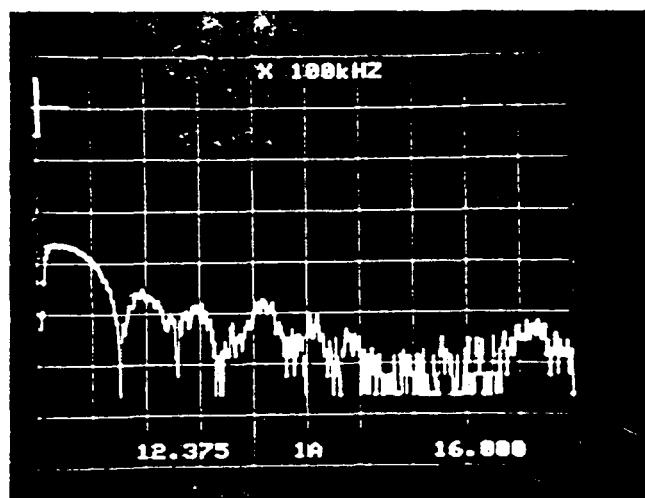
Vertical scale: 16 dB/Div.
Horizontal scale: 1237.5 kHz/Div.

Fig. 18 (d)   FFT - LOG plot of one impulse response signal of transducer.
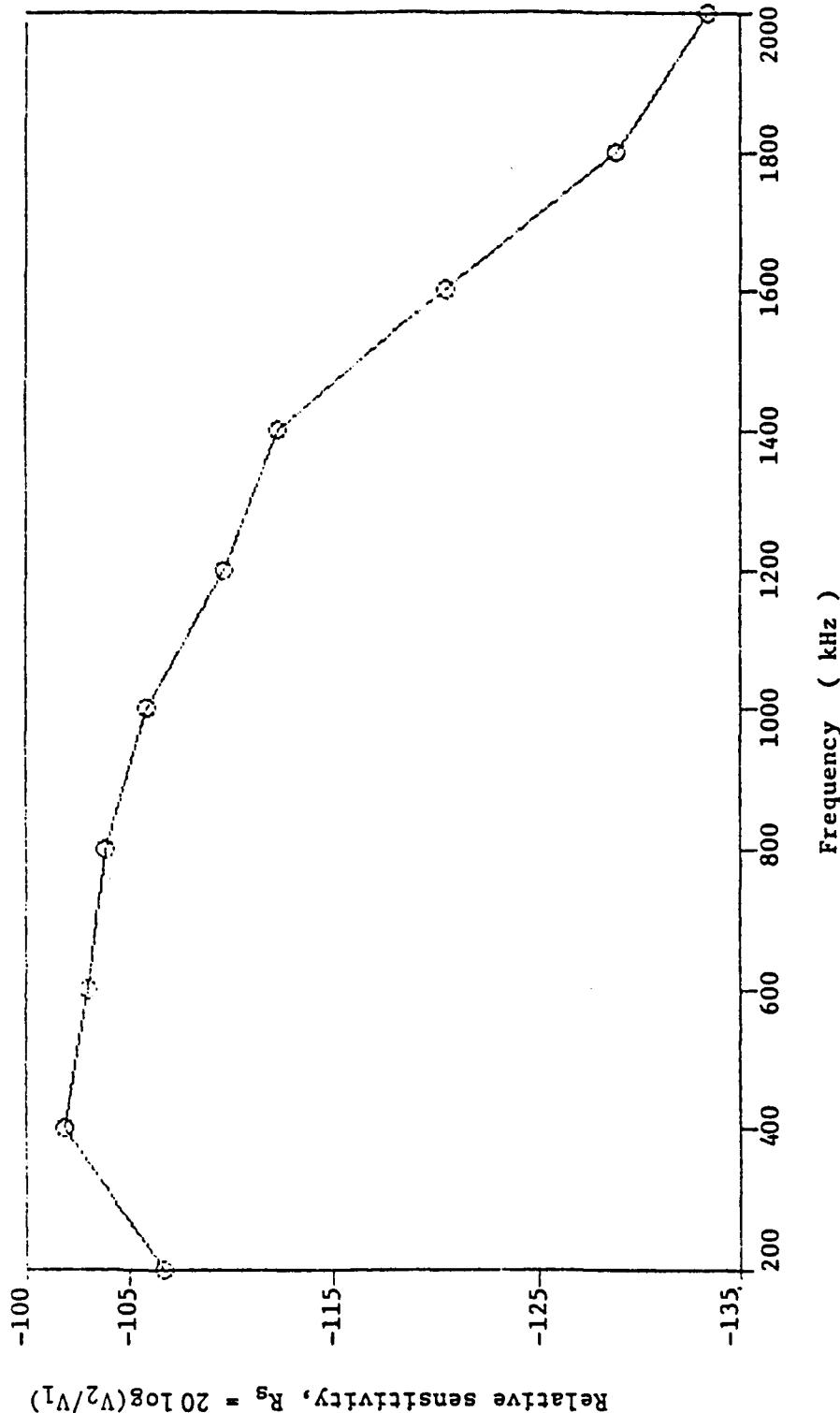
Fig. 19 Relative sensitivity versus frequency.
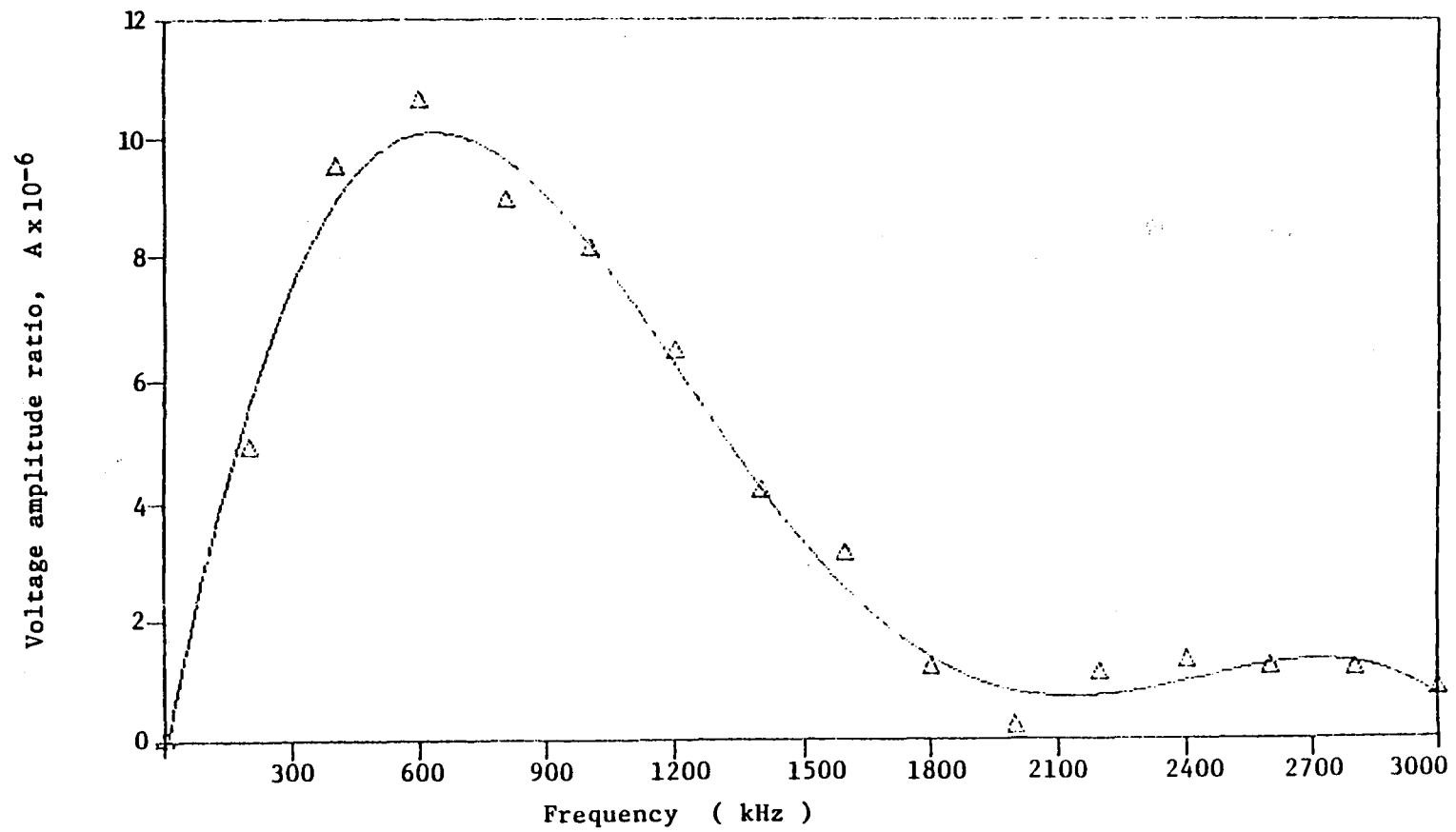
Fig. 20   Voltage amplitude ratio versus frequency obtained during non-contact characterization technique.
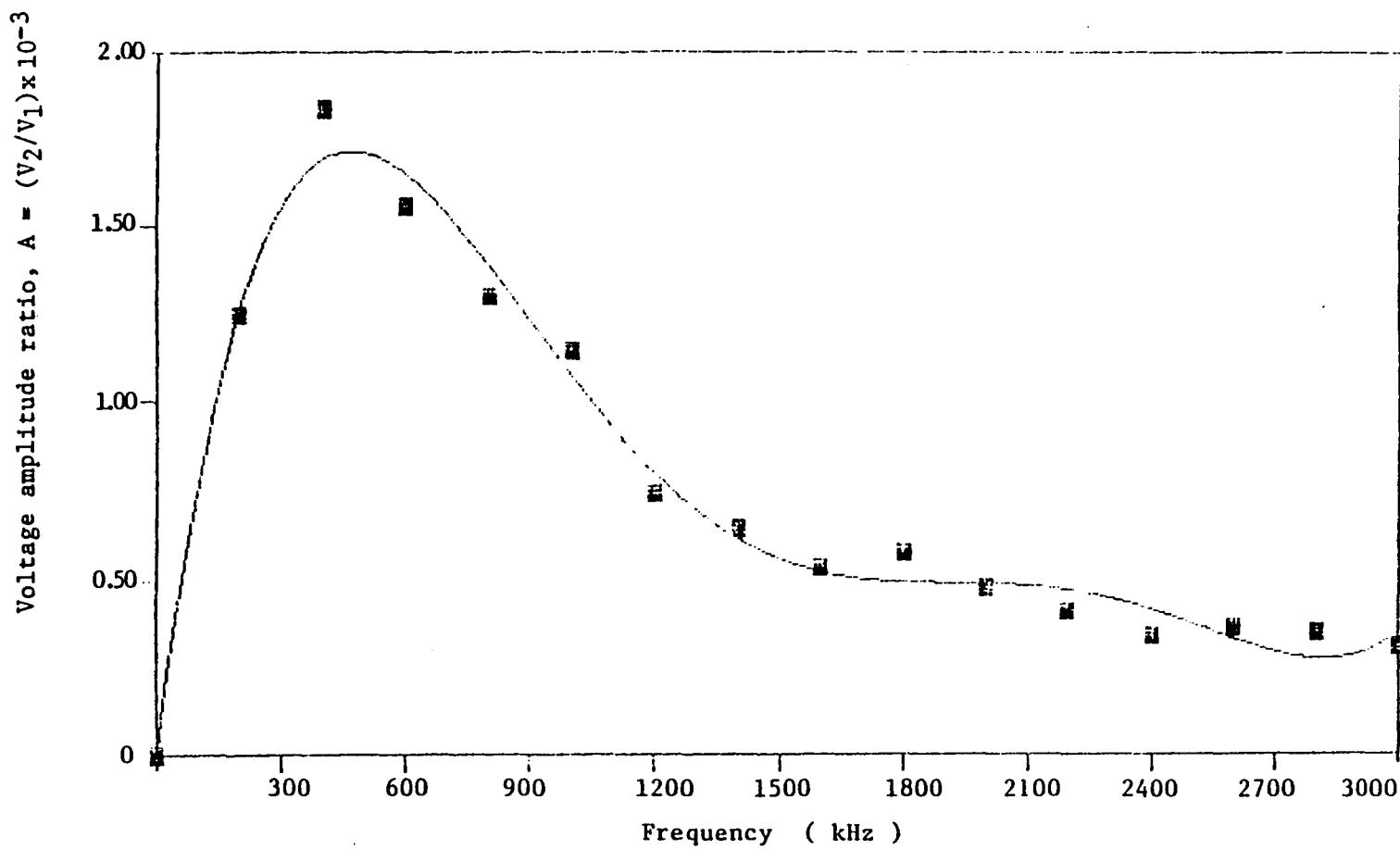
Fig. 21   Voltage amplitude ratio versus frequency obtained during tone burst characterization technique.
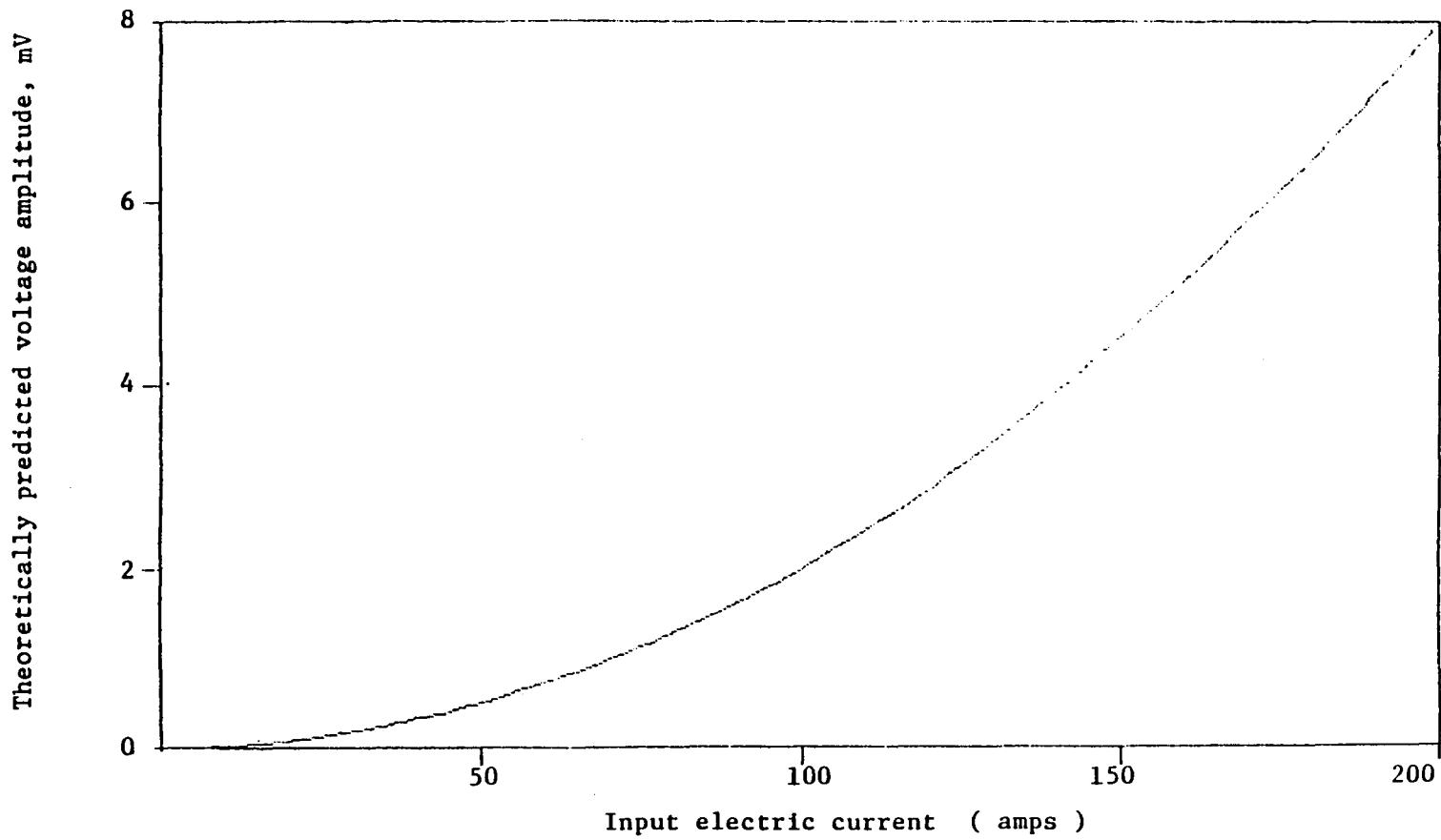
Fig. 22   Theoretically predicted output voltage versus electric current I at
conductor – piezoelement gap spacing z = 0.025in.
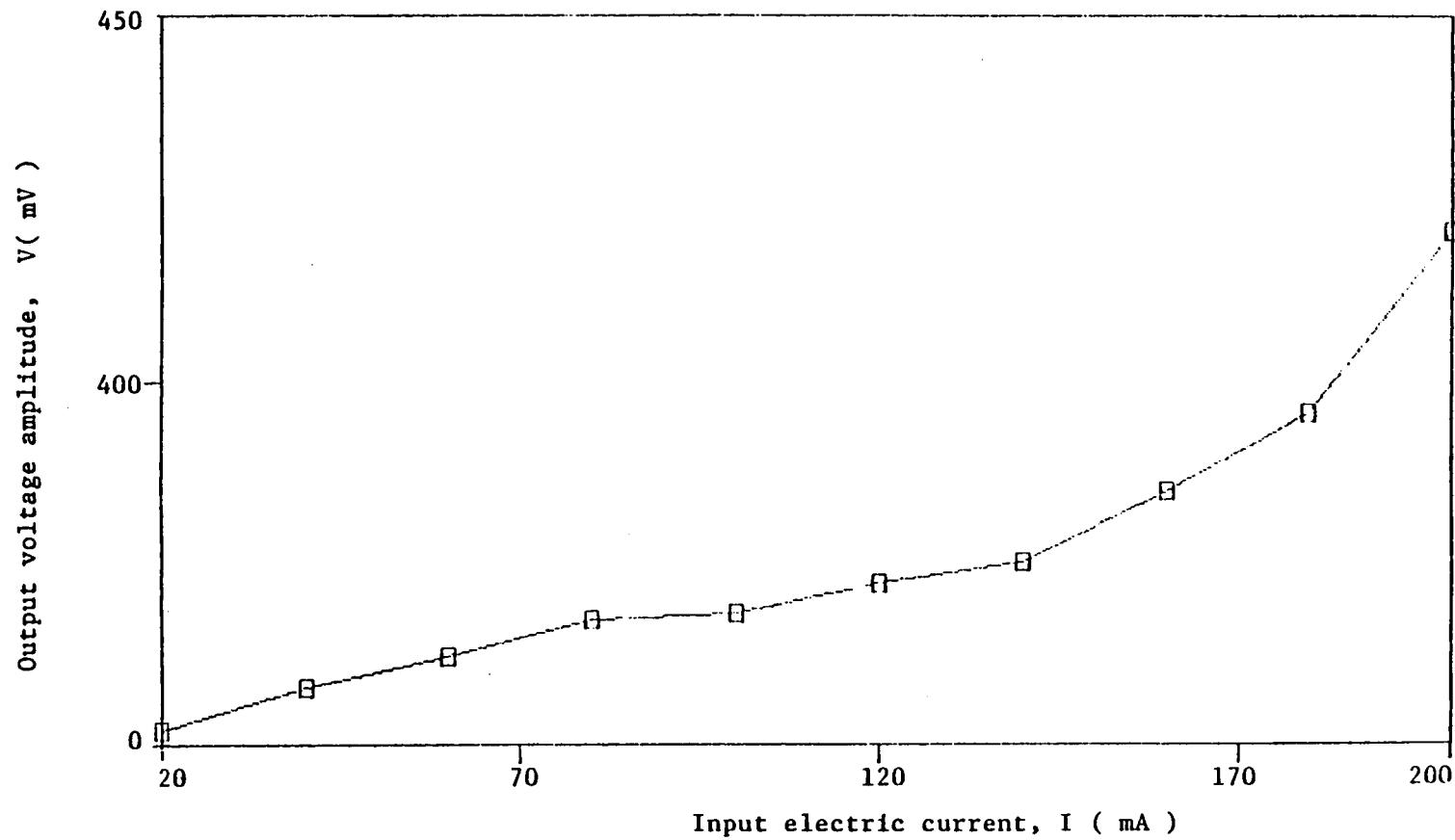
Fig. 23   Experimental output voltage amplitude versus input electric current at
conductor – piezoelement gap spacing z = 0.025in.
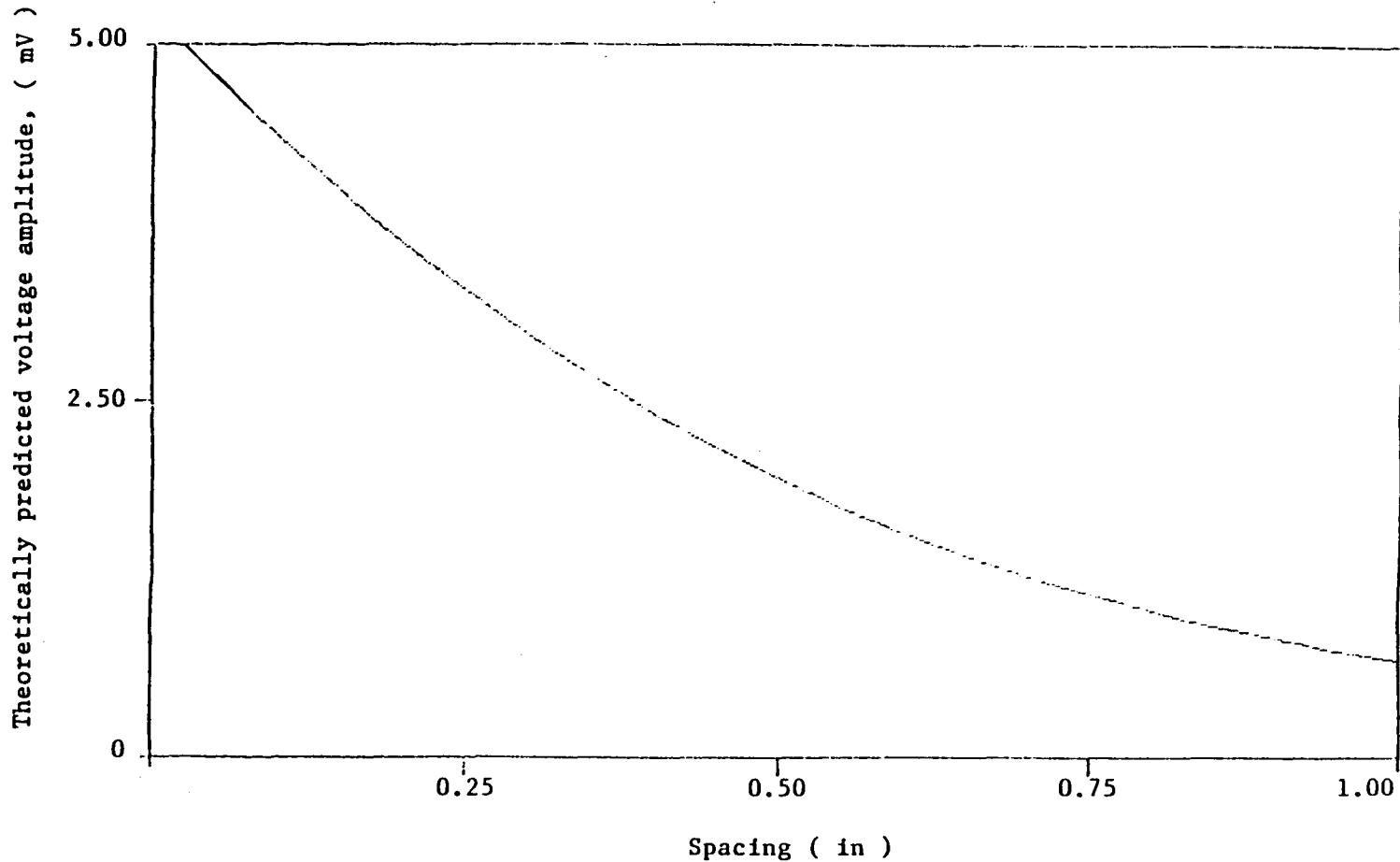
Fig. 24   Theoretically predicted voltage amplitude versus conductor - piezoelement gap spacing when input current I = 100 mA.
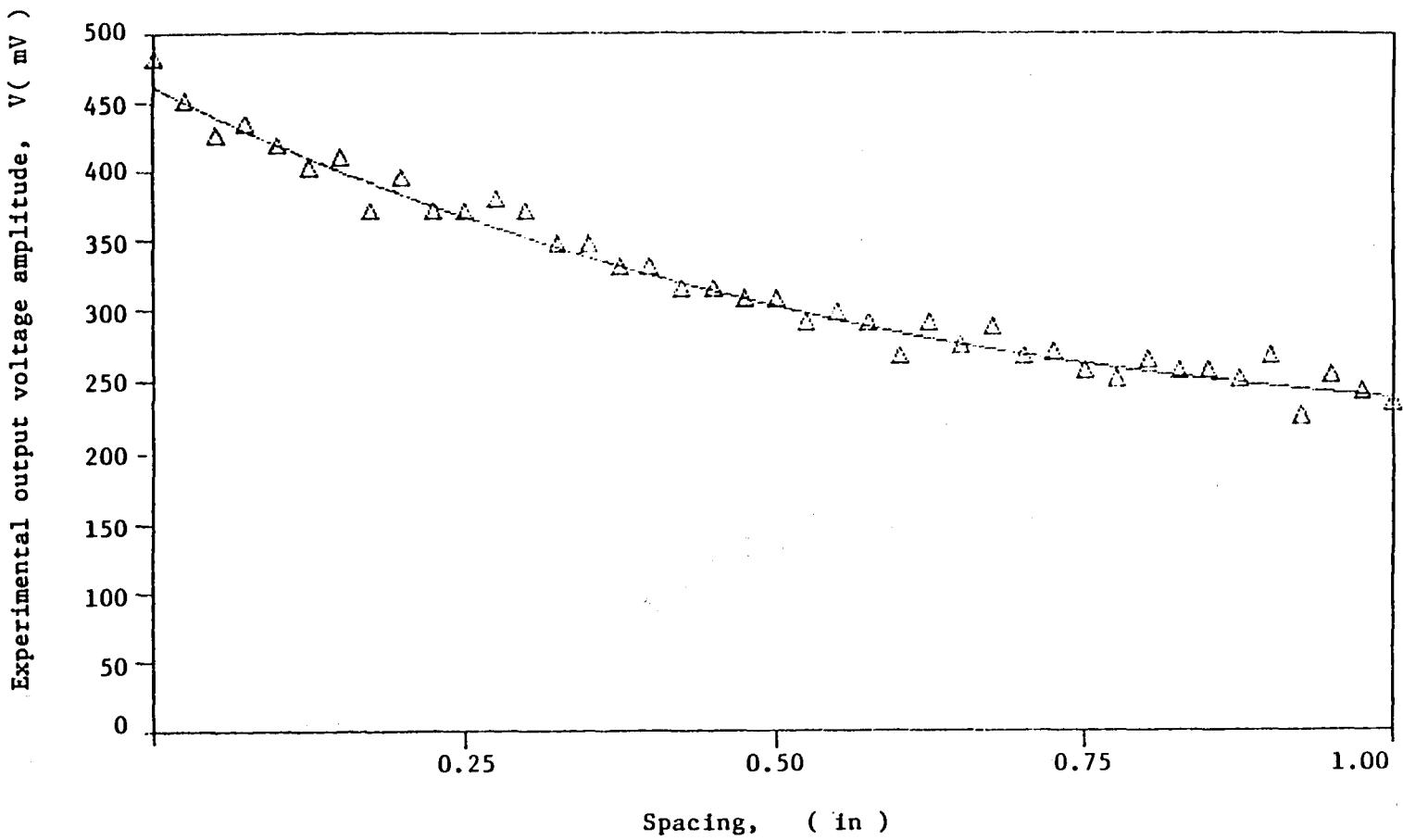
Fig. 25   Experimental output voltage amplitude versus conductor - piezoelement gap spacing when
input current I = 100 mA.
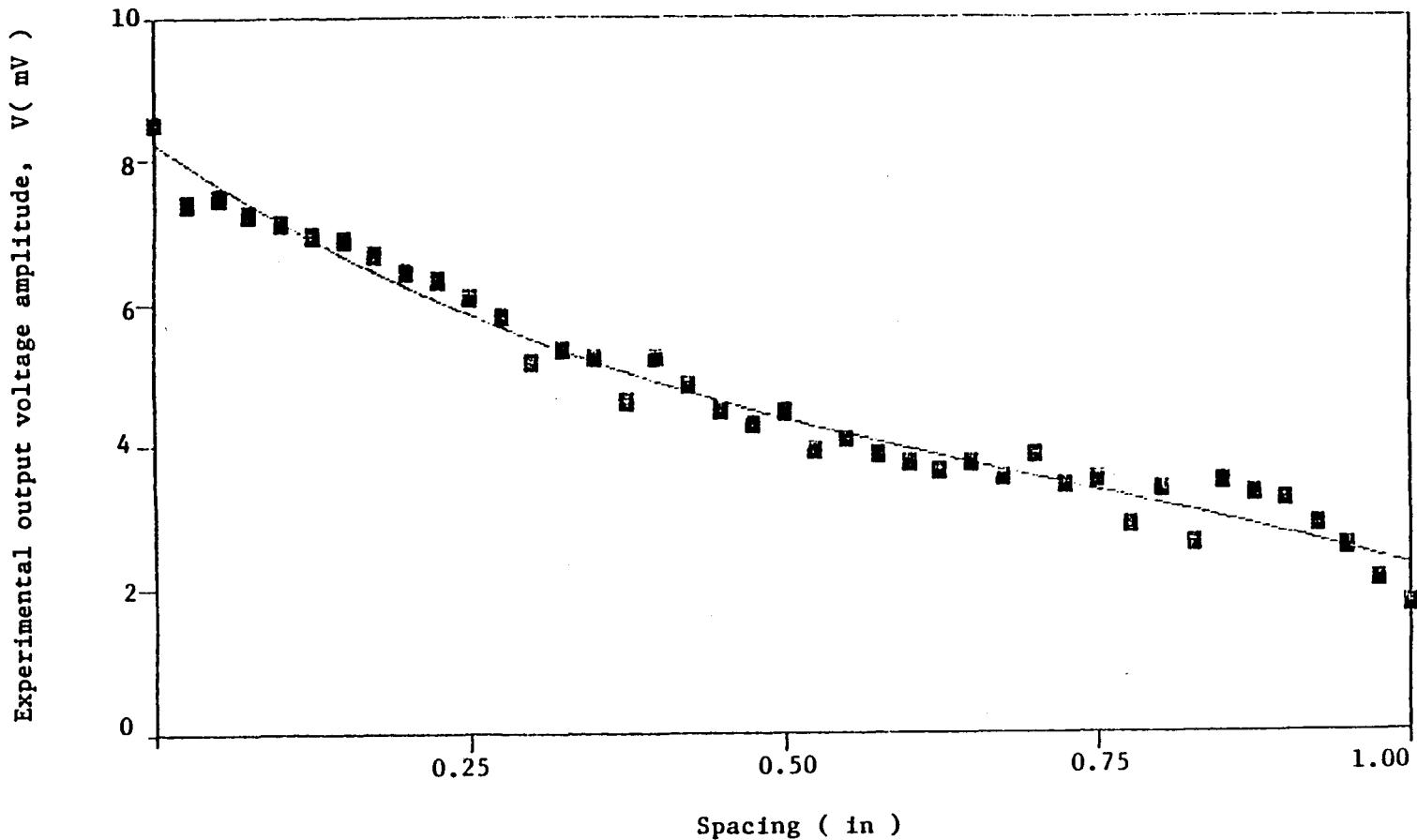
Fig. 26   Experimental output voltage amplitude (measured at central frequency f_O = 600 kHz)   versus

conductor – piezoelement gap spacing when input current I = 100 mA.

APPENDIX A

CHARACTERISTICS OF TRANSDUCER (*IQI* Model 501) BY TONE BURST TECHNIQUE

One of the standard methods for characterization of ultrasonic transducers, namely, the tone burst technique, is used here for studying the characteristic features of a dynamic surface displacement transducer (*IQI* Model 501). The technique involves the use of sweeping time-limited sine waves of varying frequencies to measure the ratio of the output signals from the transducer to the input signals. In several studies, including a recent study on piezoelectric transducers by Williams and Doll [12], the use of the technique is presented in greater detail than will be presented here. A summary of such detail can also be found in [14].

A1   TEST SPECIMEN, EXPERIMENTAL EQUIPMENT AND PROCEDURES

Test Specimen

The specimen was transducer IQI Model 501.

Experimental Equipment

A schematic of the experimental system is shown in Fig. $A1$. The system consisted of a pulsed generator (Arenberg model $PG-652C$) for generating the input sinusoidal waves; a low frequency amplifier (Arenberg LFA 550); a transmitting transducer (Acoustic Emission Technology, $V112$ longitudinal type); a transducer-specimen interface couplant ($AET\ SC-6$); a 10 inch-square aluminum (6061-$T6$) plate 1/8 in in thickness; a digital oscilloscope (Nicolet model $XF44$).

One attenuator set at 10 dB reduced the input signal to 100 volts (peak-to-peak) into the transmitting transducer. A second attenuator set at 20 dB, reduced the 100 voltage amplitude of the input signal to 10 volts at the oscilloscope only. The amplitude of the output signal from the receiving transducer was reduced by a series of other factors including the geometry of the aluminum plate. The two transducers were mounted face-to-face across the aluminum plate as shown in Fig. $A1$. The transmitting transducer was simply taped onto the plate with a scotch tape while the receiver was placed on the opposite side of the plate. The weight of the transducer IQI of 2.83 N acting on its piezoelement tip area of $7 \times 10^{-6}\,m^2$ provided a coupling pressure of $4.00 \times 10^5 N/m^2$ which exceeds a saturation pressure Of $2.5 \times 10^5 N/m^2$ which is defined as the minimum transducer-specimen interface pressure which results in the maximum amplitude of the output signal, all other parameters being constant [24]. Also, the combined weight of the aluminum plate and the transducer of 9.5 N acting on the surface area $41 \times 10^{-6} m^2$ of the transmitting transducer provided it with a coupling pressure of $2.3 \times 10^5 N/m^2$ which is close to the saturation pressure.

Experimental Procedure

The pulsed generator was set at a frquency of 200 kHz and subsequently incremented in steps of 200 kHz up to about 3000 kHz. At each frequency increment a single 100 volt peak-to-peak tone burst was input into the transmitting transducer and the resulting output signal from the receiving transducer was recorded on data diskettes. The duration of the sinusoidal input signals was chosen such that output due to to multiple reflections did not overlap.

A2   RESULTS AND DISCUSSIONS

A typical stress wave sinusoidal signal transmitted into the aluminum plate and the resulting received output signal as measured by the receiving transducer are shown in Fig. $A2$. Spectral characteristics of the transducer can be obtained by computing the ratio R_f of the received (output) signal to the input signal measured at various frequencies and plotting the values of R_f versus frequency.

The ratio R_f can therefore be expressed as

$$R_f = \left(\frac{v_2}{v_1}\right)_f \quad , \tag{A1}$$

where v_1 and v_2 are the input and output voltage amplitudes, respectively. The subscript f denotes the frequency at which each measurement is performed.

Based on eqn.(A1), a plot of R_f versus frequency was obtained as shown in Fig. $A3$. Some of the characteristic features of the transducer such as

(a) the central frequency which is usually denoted by f_0,

(b) the quality factor denoted by Q, and

(c) the flat amplitude response range were deduced from the plot. The central frequency f_0 was found to be 580 kHz while Q was calculated to be approximately 0.85. The flat amplitude response ranged from about 200 kHz to 1200 kHz.

Next, the phase angles between the input and the output signals were computed and plotted versus frequency from 200 kHz to 2000 kHz. This frequency range was selected so as to correspond to the frequency range where dominant voltage amplitudes were received by the transducer.

In order to calculate the phase angle between the input and output signals, consider schematics of the input and output sinusoidal waves as shown in Fig. A4. Assuming that the input wave has no phase shift, then the expression for the input wave can be written as

$$v_1 = a_1 \sin \omega t \quad , \tag{A2}$$

78

where a_1 is the amplitude of the input wave. Also, assuming that the phase angle between the input and output waves is ϕ, then the expression for the output signal can be witten as

$$v_2 = a_2 \sin(\omega t - \phi) \quad, \tag{A3}$$

where a_2 is the amplitude of output wave. For point B on the output wave the expression for v_2 can be expressed as

$$v_2\left(\frac{\pi}{2\omega} + \Delta t\right) = a_2 \tag{A4}$$

where Δt is the time difference between the output and input waves or between points A and B as shown in Fig. A4. Eqn. (A4) can be rewritten as

$$a_2 \sin\left(\omega\left(\frac{\pi}{2\omega} + \Delta t\right) - \phi\right) = a_2 \tag{A5}$$

So, from eqn.(A5), it can deduced that

$$\pi/2 + \omega\Delta t - \phi = \pi/2 \tag{A6}$$

Finally, the phase angle $\phi(\omega)$ between the input and output signals can be expressed as

$$\phi(\omega) = \omega t_2 \quad, \Delta t = t_2 \tag{A7}$$

where t_2 [sec] is the time at which the output wave commences which is equal to the time-shift between the two waves Δt, ω [rad/sec] is the circular frequency of the two waves and $\phi(\omega)$ [radians] is the phase angle between the input and output signals.

In the actual experimental measurements a phase angle between the input and output occurs first of all because of the time required for the stress waves to travel from the transmitting transducer through the aluminum plate to the receiving transducer. Subtracting the first effect requires that t_2 be shifted backwards with a time t_s which is given by

$$t_s = t_2 - t_a \quad, \tag{A8}$$

79

where t_a is the transmit time through the aluminum plate.

With this in mind and based on eqn.(A7), a curve which relates $\phi(\omega)$ to the various frequencies was generated and is shown Fig. $A5$. Three observations can be made from the plot:

(a) Within the flat amplitude response range of the transducer, that is, between 200 kHz and 1200 kHz, the phase angle varies between approximately +1 and -1 radians.

(b) A phase change occurs at about 580 kHz which is within 80 kHz of the central frequency.

(c) Above 1200 kHz, the phase angle varies between -1 and -3.5 radians. The behavior of the transducer based on the above observations compares favorably with that recorded for a standard conical transducer with flat sensitivity range between 100 kHz to 1000 kHz as presented in a paper by Proctor [30].

An ideal transducer would have contant amplitude and constant phase within its flat frequency response range. This is not the case in practice as is illustrated in this study. The departure of the phase from this ideal value represents one imperfection of the transducer and this is also reflected in the accuracy of the transducer on measurements.
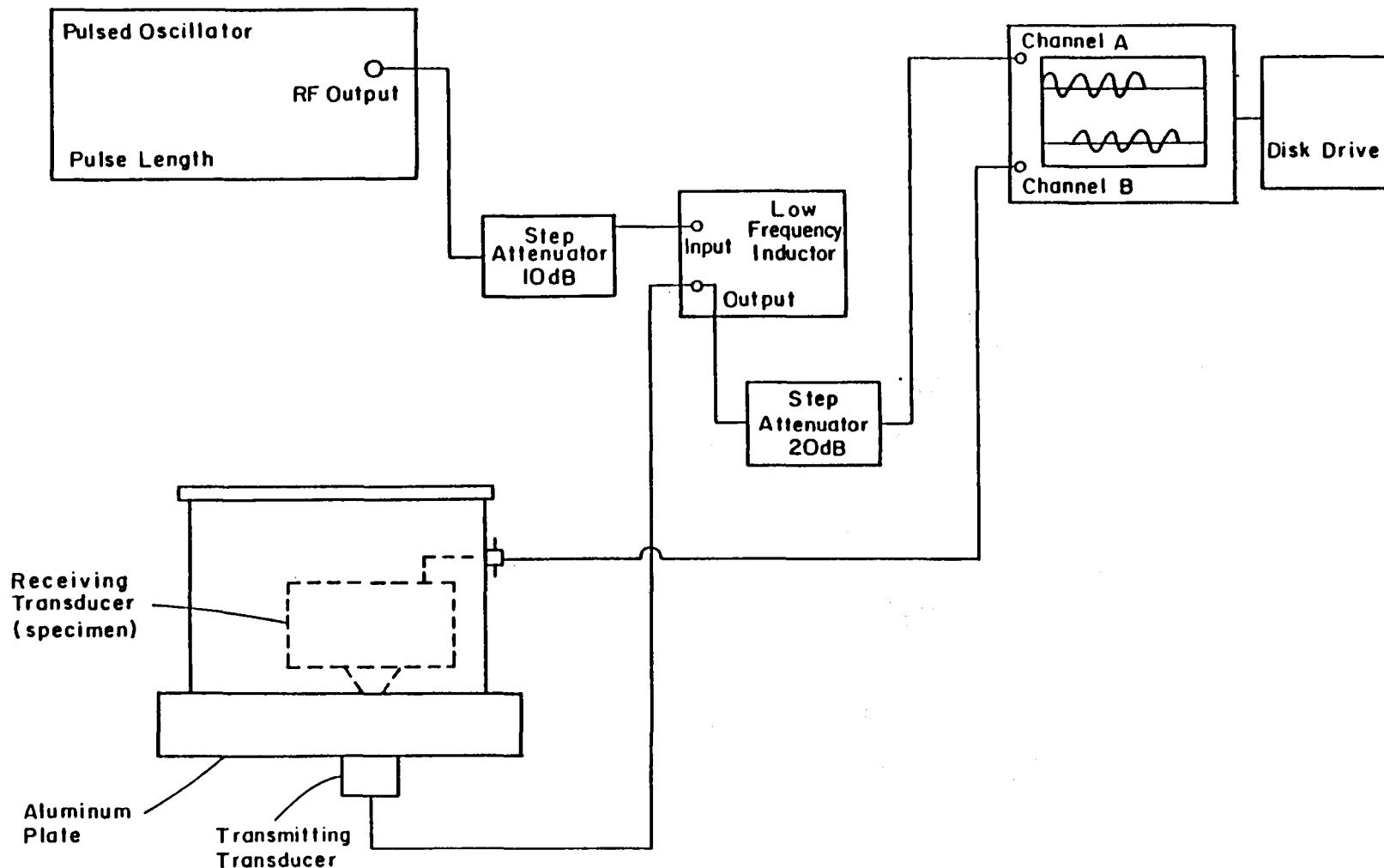
Fig. A1   Schematic of measuring equipment.
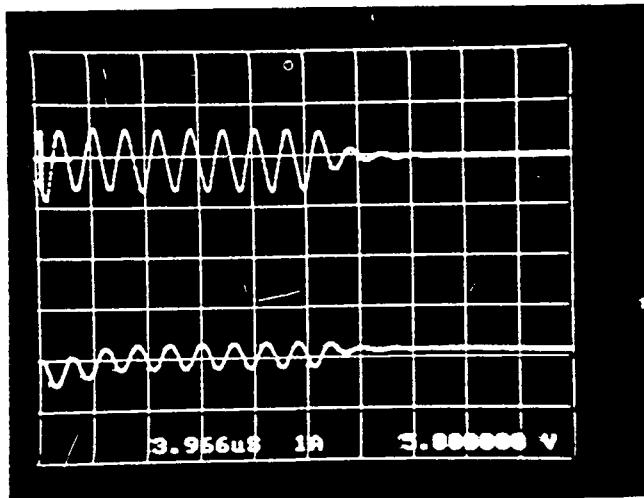
Input trace

Vertical scale: 5 V/Div.

Horizontal scale: 3.966 μs/Div.

Output trace

Vertical scale: 250 mV/Div.

Horizontal scale: 3.966 μs/Div.

Fig. A2   Input and output signals measured at 600 kHz center frequency.
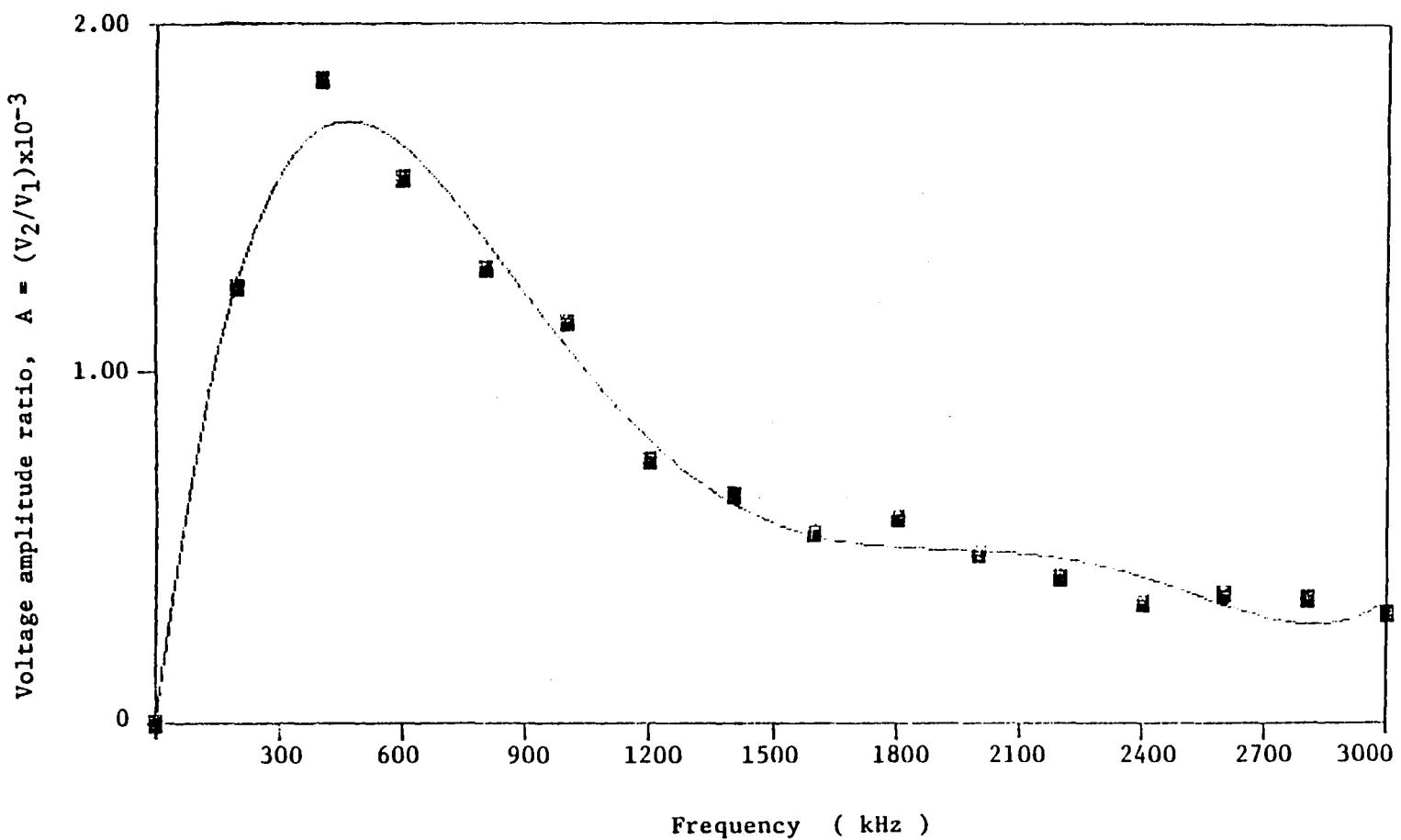
Fig. A3   Voltage amplitude ratio   versus   frequency obtained during tone burst characterization technique.
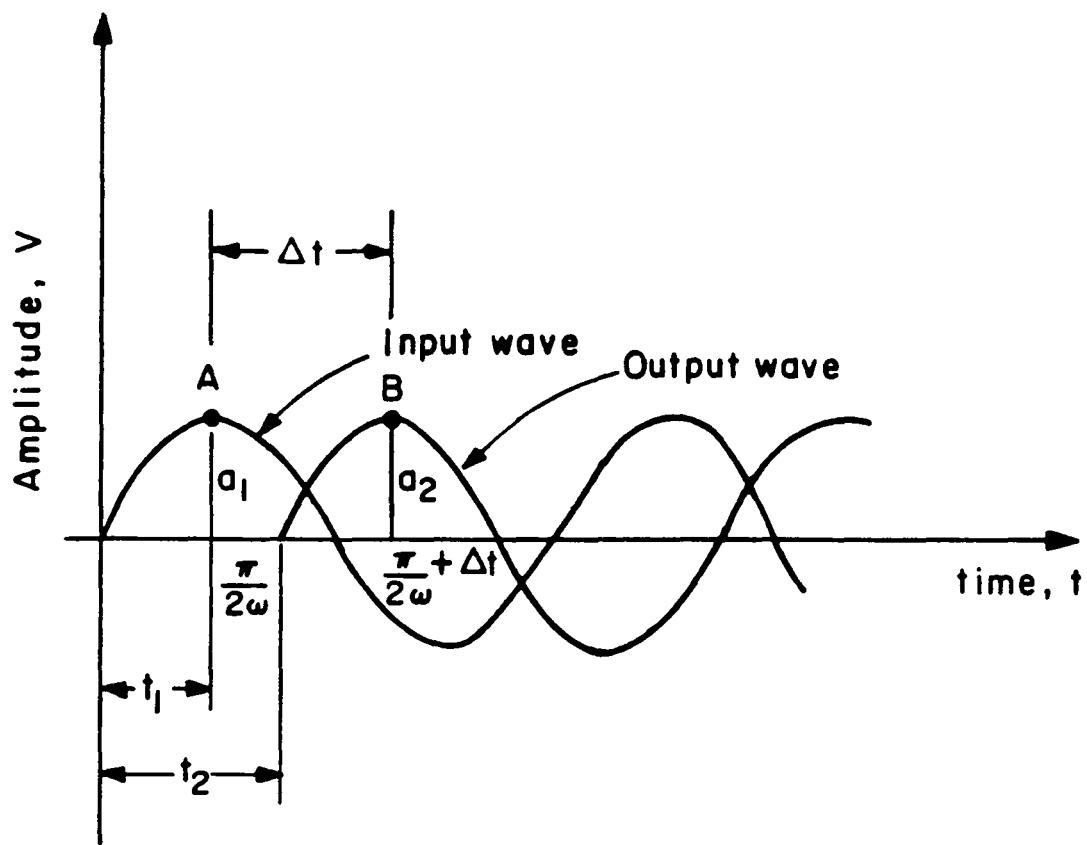
Fig. A4   Schematics of input and output sinusoidal waves propagating at same frequency but with phase angle difference.
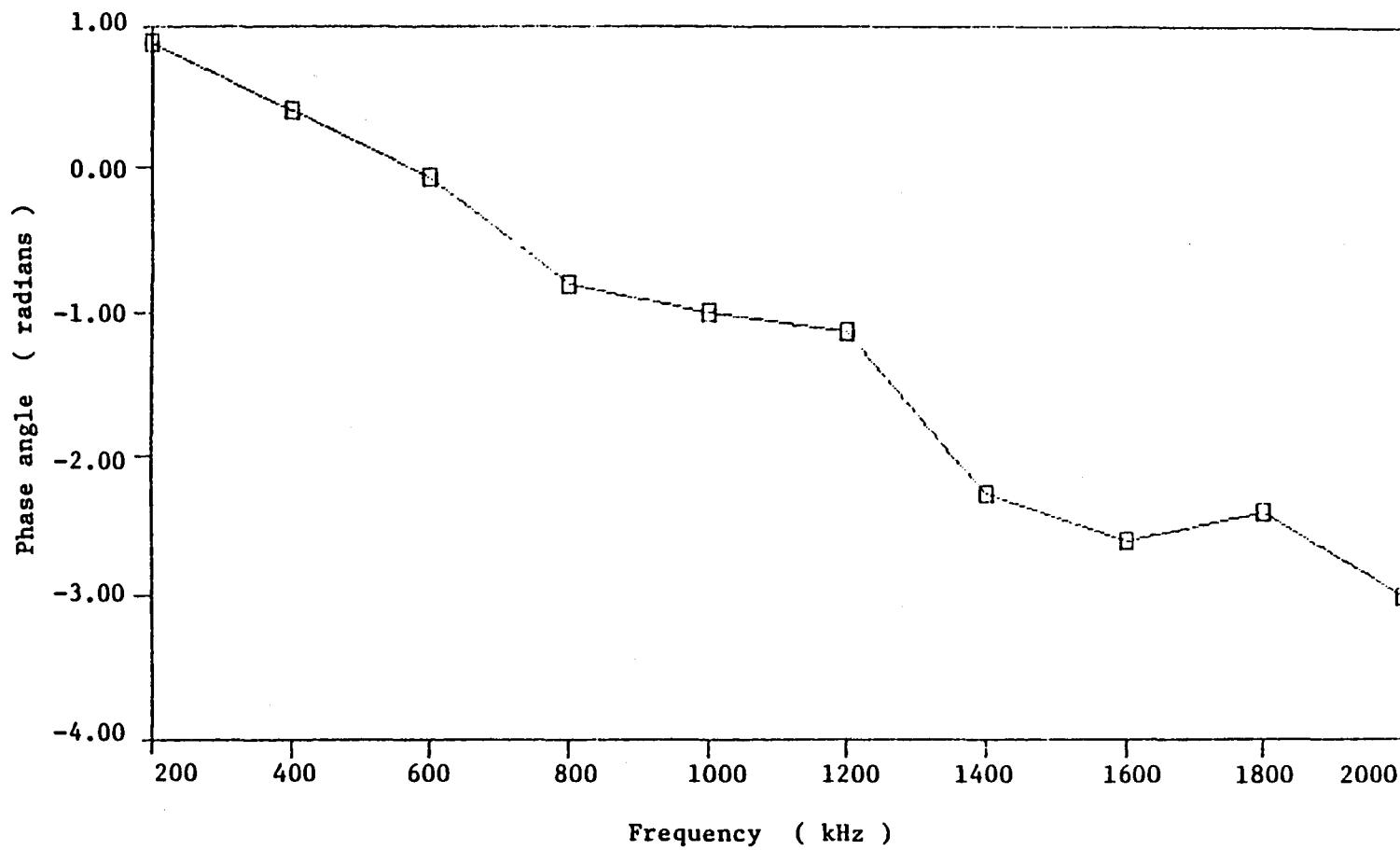
Fig. A5   Phase angle versus frequency obtained by tone burst technique.

NASA
National Aeronautics and
Space Administration

Report Documentation Page

1. Report No.	2. Government Accession No.	3. Recipient's Catalog No.
NASA CR-4151		

4. Title and Subtitle	5. Report Date
Characterization of Noncontact Piezoelectric Transducer With Conically Shaped Piezoelement	June 1988
	6. Performing Organization Code

7. Author(s)	8. Performing Organization Report No.
James H. Williams, Jr., and Simeon C.U. Ochi	None (E-3995)
	10. Work Unit No.
	506-43-11

9. Performing Organization Name and Address	11. Contract or Grant No.
Massachusetts Institute of Technology Department of Mechanical Engineering Cambridge, Massachusetts 02139	NAG3-328
	13. Type of Report and Period Covered

12. Sponsoring Agency Name and Address	
National Aeronautics and Space Administration Lewis Research Center Cleveland, Ohio 44135-3191	Contractor Report
	14. Sponsoring Agency Code

15. Supplementary Notes

16. Abstract

In this report, the characterization of a dynamic surface displacement transducer (IQI Model 501) by a noncontact method is presented. The transducer is designed for ultrasonic as well as acoustic emission measurements and, according to the manufacturer, its characteristic features include: a flat frequency response range which is from 50 to 1000 kHz and a quality factor Q of less than unity. The characterization is based on the behavior of the transducer as a receiver and involves exciting the transducer directly by transient pulse input stress signals of quasi-electrostatic origin and observing its response in a digital storage oscilloscope. Theoretical models for studying the response of the transducer to pulse input stress signals and for generating pulse stress signals are presented. The characteristic features of the transducer which include the central frequency f_o, quality factor Q, and flat frequency response range are obtained by this noncontact characterization technique and they compare favorably with those obtained by a tone burst method which are also presented.

17. Key Words (Suggested by Author(s))	18. Distribution Statement
Nondestructive testing, Nondestructive evaluation; Transducers; Ultrasonic; Acoustic emission; Noncontact ultrasonics; Piezoelectric effect; Transducer characterization	Unclassified – Unlimited Subject Category 38

19. Security Classif. (of this report)	20. Security Classif. (of this page)	21. No of pages	22. Price*
Unclassified	Unclassified	87	A05

End of Document